

Effective theory approach to direct detection of dark matter

Junji Hisano

*Kobayashi-Maskawa Institute for the Origin of Particles and the Universe,
Nagoya University, Nagoya 464-8602, Japan*

Department of Physics, Nagoya University, Nagoya 464-8602, Japan

*Kavli IPMU (WPI), UTIAS, The University of Tokyo, Kashiwa,
Chiba 277-8583, Japan*

Abstract

An effective field theory approach is presented for evaluation of the dark matter direct detection rate in this lecture note. This is prepared for the Les Houches Summer School Effective Field Theory in Particle Physics and Cosmology, July 2017.

1 Introduction

There is now no doubt that dark matter (DM) exists in the universe. However, we do not know the nature of the DM, since our knowledge about DM is limited to the gravitational aspect. We have no DM candidates in the standard model (SM) of particle physics and also in astronomy, and the DM is now one of the big issues in physics. The idea that DM may be unknown particles produced in the early universe is fascinating, and many candidates for the DM have been proposed [1]. Weakly-Interacting Massive Particles (WIMPs) are one of the leading candidates. They are assumed to be produced in the thermal bath in the early universe. The typical WIMP mass scale is $O(100)$ GeV to $O(1)$ TeV under this assumption. We also expect new physics beyond the SM at the TeV scale from the naturalness point of view. This coincidence is called the WIMP miracle. Many experiments now search for WIMP DM. Direct detection of WIMP DM on Earth is one of the methods. The WIMPs are assumed to pass through us. For example, about one million WIMPs may exist in this room. Their interactions are very weak, though there is a small probability that they may collide with nuclei. Direct detection experiments observe the recoiled nuclei. Many such experiments are currently working or have been proposed. A recent review of direct detection experiments is, for example, given in Ref. [2].

In this lecture, the WIMP DM detection rate from UV theories at the TeV scale is evaluated. In this evaluation, the effective theory approach works well. UV theories provide the interactions of WIMPs with partons. On the other hand, we need to know the effective interactions of WIMPs with nuclei. We have to derive effective theories at the parton, nucleon, and nuclei levels. In this lecture, we note the QCD aspects in the evaluation of WIMP interactions with nucleons. We will show that we can handle QCD corrections to the Wilson coefficients in the effective interactions at the parton level well. We may then evaluate the next-leading order contribution of α_s , and the strategy for the evaluation will be shown.

The lecture notes are organized as follows. First, we give an introduction to the WIMP DM. After discussing the effective interactions of WIMPs with nuclei and nucleons in Section 3, we give a brief review of the direct detection experiments in Section 4. Then, we will show how to evaluate the effective interactions of WIMPs with nucleons from UV theories in Section 5. Due to the nucleon matrix elements of the parton-level effective operators, the power counting of α_s in calculating the direct detection rate is not the same as in conventional ones. Furthermore, we do not necessarily need to evaluate the Wilson coefficients for parton-level effective operators at the hadronic scale with renormalization-group (RG) equations, in contrast to the hadronic observables in flavor physics. These topics are discussed in this section. In Section 6 we show some results for three UV models as examples: 1) gauge singlet WIMPs coupled with the Higgs boson, 2) gauge singlet WIMPs coupled with colored scalars and quarks, and 3) $SU(2)_L$ non-singlet WIMPs. We assume that the WIMPs are Majorana fermions in this lecture. The application to other WIMPs is straightforward. Finally, we discuss the strategy to evaluate the direct detection rate including the $O(\alpha_s)$ correction in Section 7. Section 8 is devoted to the Summary. In Appendix A we introduce Fock–Schwinger gauge fixing, which is quite

useful in evaluating the Wilson coefficients of the effective operators including gluon field strengths. This lecture is mainly based on the author’s recent works [3, 4].

2 WIMP DM

If the DM is composed of unknown particles, they are electrically neutral. They are stable, or have a longer lifetime than the age of the universe. They are massive so that they are “cold” in the structure formation era of the universe, i.e., the free streaming length after production in the early universe is shorter than the size of protogalaxies so that the small-scale structure in the universe is not erased. The cold DM abundance is precisely determined from CMB power spectrum measurements. The DM particles are nonrelativistic in the current universe, and the energy density ρ_X is given by $M_X n_X$, with M_X and n_X the DM particle mass and number density, respectively. It has been found from the CMB measurements that the DM energy density normalized by the critical density in the universe, $\Omega_X \equiv \rho_X / \rho_{\text{critical}}$, is about 27% [5]. The critical density is $\rho_{\text{critical}} \simeq 10^{-5} \text{GeV}/\text{cm}^3$. The abundance and the free streaming length depend on the production mechanism in the early universe. In WIMP scenarios, the WIMPs are assumed to be in thermal equilibrium in the early hot universe.

One of the representative models for WIMPs is the supersymmetric standard model (SUSY SM) [6]. In this model, a Z_2 symmetry called the R -parity is introduced, in order to stabilize protons. As the result, the lightest SUSY particle is stable. The neutral components of the fermionic superpartners of the gauge and Higgs bosons, called gauginos and Higgsinos, are WIMP candidates in the SUSY SM. Another representative model is the universal extra dimension (UED) model [7]. In this model, we can impose a parity symmetry in extra dimensional space, and the lightest Kaluza–Klein particle is stable [8]. The candidate in the minimal model is the Kaluza–Klein photon. The SUSY SM and the UED model are motivated by the naturalness problem in the Higgs boson mass term in the SM so that their energy scale is expected to be at the TeV scale. As will be explained below, the WIMPs have masses of about $O(100) \text{ GeV}$ – $O(1) \text{ TeV}$ if they were produced in the thermal bath in the early universe. These two observations support the assertion that new physics will appear at the TeV scale. Many models have been proposed in order to explain the naturalness and the WIMP DM.

Now, we evaluate the WIMP DM abundance in the universe. In the WIMP scenarios, the WIMPs have interactions with the SM particles so that the WIMPs are thermalized in the early hot universe. The stability of the WIMPs comes from global symmetries, as given in the above examples. In the early universe, where the temperature (T) is much higher than the WIMP mass (M_X), they are in thermal equilibrium, and the number density is comparable to those for the SM particles. When the temperature decreases to below the WIMP mass, WIMP pair production by SM particle collisions is suppressed in the thermal bath, so that the WIMP number density deviates from that in thermal equilibrium. The WIMP pair annihilation is frozen when the WIMPs do not find partners for their pair annihilation within a Hubble time, and the number density is only diluted

by the expansion of the universe. Thus, the current abundance of WIMPs is determined by the WIMP pair annihilation cross section.

The WIMP abundance is more precisely evaluated with the Boltzmann equation [9],

$$\frac{dn_X}{dt} + 3H(T)n_X = -\langle\sigma|v|\rangle \left[n_X^2 - (n_X^{\text{EQ}})^2 \right]. \quad (1)$$

The second term is for dilution due to the expansion of the universe. The Hubble parameter $H(T)$ in the radiation-dominated (RD) era is given by

$$H(T) = \sqrt{\frac{8\pi}{3M_{\text{pl}}}\rho} \simeq \sqrt{\frac{4\pi}{45}g_\star^{1/2}} \frac{T^2}{M_{\text{pl}}} \quad (2)$$

where M_{pl} is the Planck mass and ρ is the energy density ($\rho = (\pi^2/30)g_\star T^4$ with $g_\star = \sum_{\text{boson}} 1 + \sum_{\text{fermion}} 7/8$). If the collision term in the right-hand side of the Boltzmann equation is zero, n_X/s (s is the entropy density, $s = (2\pi^2/45)g_\star T^3$) is constant since s is also diluted by the expansion of the universe. In the collision term, $\langle\sigma|v|\rangle$ is the thermal-averaged WIMP pair annihilation cross section and n_X^{EQ} is the WIMP number density in thermal equilibrium. The collision term is proportional to the square of the WIMP number density since it comes from the WIMP pair annihilation and production.

The Boltzmann equation is rewritten as

$$\frac{x}{Y_{\text{EQ}}} \frac{dY}{dx} = -\frac{\Gamma_A}{H} \left[\left(\frac{Y}{Y_{\text{EQ}}} \right)^2 - 1 \right] \quad (3)$$

by defining Y and x as $Y \equiv n_X/s$ and $x = M_X/T$, respectively. Here, Γ_A is the probability of annihilation per unit time for a WIMP,

$$\Gamma_A = n_X^{\text{EQ}} \langle\sigma|v|\rangle. \quad (4)$$

When $x \gtrsim 1$, the WIMP pair production is kinematically suppressed, and they start to be decoupled from the thermal bath so that $Y/Y_{\text{EQ}} \gtrsim 1$. When $H \gg \Gamma_A$, the annihilation is frozen and Y becomes constant. The freeze-out temperature (T_F) and the WIMP number density at T_F (n_X^F) are approximately determined by $H(T_F) = \Gamma_A$, and it is found that T_F is about $M_X/20$ and $n_X^F \simeq H(T_F)/\langle\sigma|v|\rangle$. Thus, Y and Ω_X are approximately evaluated as

$$\begin{aligned} Y &\simeq \sqrt{\frac{45}{\pi}} g_\star^{-1/2} \frac{1}{T_F M_{\text{pl}}} \frac{1}{\langle\sigma|v|\rangle}, \\ \Omega_X &= \frac{s^{\text{now}}}{\rho_{\text{critical}}} M_X Y \simeq 0.4 \times \left(\frac{x_F \equiv M_X/T_F}{20} \right) \left(\frac{\langle\sigma|v|\rangle}{10^{-9} \text{GeV}^{-2}} \right)^{-1}, \end{aligned} \quad (5)$$

where s^{now} is the entropy density in the current universe ($s^{\text{now}} \simeq 3000 \text{cm}^{-3}$).

Let us discuss some typical cases. When the WIMPs are $\text{SU}(2)_L$ singlet fermions, the annihilation cross section into SM fermions is given by $\sigma v \sim \pi \alpha^2 M_X^2 / M_S^4$, with M_S the

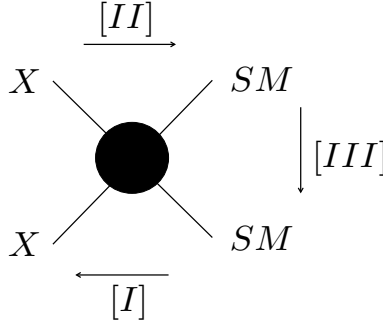


Figure 1: Three approaches to WIMP searches.

mediator scalar mass. Assuming that the mediator coupling constant α is the same as that of the $U(1)_Y$ gauge interaction, $\sigma v \sim 3 \times 10^{-9} \text{GeV}^{-2}$ for $M_X = M_S = 300 \text{GeV}$. If the mediator mass is heavier than the WIMP mass, the cross section is suppressed by $(M_X/M_S)^4$. If the WIMPs are Majorana fermions, the annihilation into SM fermions suffers from p -wave suppression so that the thermally averaged cross section is more suppressed by $T_F/M_X \sim 1/20$ or the square of the masses of the SM fermions in the final states. Thus, if the WIMPs are $SU(2)_L$ singlet Majorana fermions, the WIMP mass is around 100 GeV. Binos (the fermionic superpartners of the $U(1)_Y$ gauge boson in the SUSY SM) are an example. They are $SU(2)_L$ singlet Majorana fermions. This situation may be changed when some new particles are degenerate with the WIMPs in mass so that co-annihilation occurs [10]. For example, if staus, which are the bosonic superpartners of the tau lepton, are degenerate with the binos in mass, heavier binos are predicted due to their co-annihilation.

On the other hand, if the WIMPs are the neutral component of the $SU(2)_L$ multiplet(s), they annihilate into two weak gauge bosons. The annihilation cross section is approximately given by $\sigma v \sim \pi \alpha_2^2 / M_X^2 = 3.5 \times 10^{-9} \text{GeV}^{-2} \times (M_X/1 \text{TeV})^{-2}$. Thus, the WIMP mass is expected to be at the TeV scale. Higgsinos, which are the fermionic superpartners of Higgs bosons in the SUSY SM, are $SU(2)_L$ doublets, and winos, which are those of $SU(2)_L$ gauge bosons, are $SU(2)_L$ triplets. Detailed calculations show that the $SU(2)_L$ doublet and triplet fermion masses are about 1 TeV and 3 TeV, respectively, if they are in thermal equilibrium in the early hot universe [11].

Many kinds of experiments are currently searching for WIMPs in addition to signature of new physics at the TeV scale. The first are direct searches for WIMPs in collider experiments, such as in the LHC. (See [I] in Fig. 1.) While WIMPs do not leave any signatures in detectors in the experiments, their momenta appear missing in their events. LHC experiments are now searching for events with missing transverse momenta. The production cross sections of colored particles are larger than the those for WIMPs at the LHC, and WIMPs are mainly produced from the decay of the colored particles if they have interactions.

The second approach is indirect detection of WIMP DM in cosmic rays ([II] in Fig. 1).

WIMPs are gravitationally accumulated in massive astrophysical objects, such as stars, galaxies, and galactic clusters. The WIMP pair annihilation is increased around these objects since the annihilation rate is proportional to the square of the WIMP density. The final states in the annihilation include gamma rays, positrons, anti-protons, neutrinos, and so on, and they contribute to cosmic rays. The Fermi satellite is observing gamma rays, and it gives constraints on WIMP annihilation from observations of gamma rays from the galactic center [12] or dwarf galaxies [13]. The atmospheric Cherenkov telescopes, such as HESS and MAGIC, are also searching for gamma rays from WIMP annihilation [14]. AMS-02 on the International Space Station is searching for antiparticles [15]. The ICECUBE [16] and Super-Kamiokande experiments [17] observe solar neutrinos to place constraints on WIMP annihilation in the Sun. If non-standard signatures are found in cosmic rays, they may be interpreted as WIMP annihilation. The indirect detection is sometimes challenging due to the astrophysical backgrounds, though it may be sensitive to heavy WIMPs with masses above the TeV scale. In particular, the annihilation cross sections of $SU(2)_L$ non-singlet WIMPs are enhanced by the attractive force in weak interactions, called the Sommerfeld effect [18].

The third one is direct detection of WIMP DM trapped within our galaxy ([III] in Fig. 1). In these experiments, recoiled nuclei are observed in elastic scattering with WIMPs, $X + N \rightarrow X + N$. The typical recoil energy is $\sim m_r^2/m_T v^2$ ($m_r (= m_T M_X/(m_T + M_X))$: reduced mass, m_T : target nucleus mass, and v : DM velocity in the lab frame). The typical DM velocity around the Earth is about $10^{-3}c$ (c : speed of light). Thus, the recoil energy is (1 – 100) keV. Currently, 1 ton-class detectors, such as XENON1T [19] and PandaX-II [20], are searching for WIMP DM. We will review the experiments after showing the effective interaction of the nucleus/nucleon with WIMPs.

3 Effective WIMP-Nucleus/Nucleon Interactions

Let us discuss the WIMP-nucleus effective interactions in the non-relativistic limit for elastic scattering processes,

$$X(\vec{p}) + N(\vec{k}) \rightarrow X(\vec{p}') + N(\vec{k}'), \quad (6)$$

where \vec{p} and \vec{p}' (\vec{k} and \vec{k}') are the incoming and outgoing WIMP (nucleus, N) three-momenta, respectively. We assume that the WIMPs have spin S_X . This discussion also applies to scalar and vector WIMPs. The effective interactions are given by operators that are constructed with four vectors, the momentum transfer $\vec{q}(\equiv \vec{k} - \vec{k}')$, the incoming WIMP velocity \vec{v} , the nucleus spin \vec{S}_N , and the WIMP spin \vec{S}_X . For convenience, we introduce $\vec{P}(\equiv \vec{p} + \vec{p}' = 2\vec{p} + \vec{q})$ as an alternative to \vec{v} . In elastic scattering, $|\vec{P}|$ and $|\vec{q}|$ are proportional to v ($v \equiv |\vec{v}|$).

The effective operators are classified into two categories: (nucleus) Spin-Independent (SI) and Spin-Dependent (SD) operators. There are four SI operators [21]:

$$\begin{aligned} O_1^{(++)} &= 1, & O_2^{(-+)} &= \vec{S}_X \cdot i\vec{q}, \\ O_3^{(--)} &= \vec{S}_X \cdot \vec{P}, & O_4^{(++)} &= \vec{S}_X \cdot (\vec{P} \times i\vec{q}). \end{aligned} \quad (7)$$

Here, the superscripts ($\pm\pm$) are for the transformation properties under parity (P) and charge conjugation (C). The SD operators are the following:

$$\begin{aligned}
O_5^{(++)} &= \vec{S}_X \cdot \vec{S}_N, & O_6^{(-+)} &= \vec{S}_N \cdot i\vec{q}, \\
O_7^{(--)} &= \vec{S}_N \cdot \vec{P}, & O_8^{(--) } &= (\vec{S}_X \times \vec{S}_N) \cdot i\vec{q}, \\
O_9^{(-+)} &= (\vec{S}_X \times \vec{S}_N) \cdot \vec{P}, & O_{10}^{(++)} &= \vec{S}_N \cdot (\vec{P} \times i\vec{q}), \\
O_{11}^{(++)} &= (\vec{S}_N \cdot \vec{q})(\vec{S}_X \cdot \vec{q}), & O_{12}^{(++)} &= (\vec{S}_N \cdot \vec{P})(\vec{S}_X \cdot \vec{P}), \\
O_{13}^{(+ -)} &= (\vec{S}_N \cdot i\vec{q})(\vec{S}_X \cdot \vec{P}) + (\vec{S}_N \cdot \vec{P})(\vec{S}_X \cdot i\vec{q}) \\
O_{14}^{(+ -)} &= (\vec{S}_N \cdot i\vec{q})(\vec{S}_X \cdot \vec{P}) - (\vec{S}_N \cdot \vec{P})(\vec{S}_X \cdot i\vec{q}) \\
O_{15}^{(-+)} &= [\vec{S}_N \cdot (\vec{P} \times \vec{q})](\vec{S}_X \cdot \vec{q}) + [\vec{S}_X \cdot (\vec{P} \times \vec{q})](\vec{S}_N \cdot \vec{q}) \\
O_{16}^{(- -)} &= [\vec{S}_N \cdot (\vec{P} \times i\vec{q})](\vec{S}_X \cdot \vec{P}) + [\vec{S}_X \cdot (\vec{P} \times i\vec{q})](\vec{S}_N \cdot \vec{P}) .
\end{aligned}$$

The Wilson coefficients for these sixteen operators depend on $|\vec{q}|$. The effective interactions depending on \vec{P} and/or \vec{q} are suppressed by v . Two operators, $O_1^{(++)}$ (SI) and $O_5^{(++)}$ (SD), are dominant in the elastic scattering unless they are accidentally suppressed. In the following, we will concentrate on these cases.

The effective interactions of WIMPs with nuclei are derived from those with nucleons. When the WIMPs are Majorana fermions (X), the effective interactions with nucleons ($N = n, p$) are simple, given by*

$$L_{\text{eff}} = \sum_{N=n,p} (f_N \bar{X} X \bar{N} N + a_N \bar{X} \gamma^\mu \gamma_5 X \bar{N} \gamma_\mu \gamma_5 N) . \quad (8)$$

The first term is the SI interaction in the non-relativistic limit, while the second one is the SD one. Neglecting nucleus form factors, the elastic-scattering cross sections of WIMPs with nuclei are given by

$$\sigma = \sigma_{\text{SI}} + \sigma_{\text{SD}} \quad (9)$$

with

$$\begin{aligned}
\sigma_{\text{SI}} &= \frac{4}{\pi} m_r^2 |Z f_p + (A - Z) f_n|^2, \\
\sigma_{\text{SD}} &= \frac{16}{\pi} m_r^2 \frac{J + 1}{J} |a_p \langle S_p \rangle + a_n \langle S_n \rangle|^2.
\end{aligned} \quad (10)$$

Here, Z and A are the atomic and mass numbers, respectively, and J and $\langle S_N \rangle$ are the total spin of target nucleus and the expectation value of the nucleon spin in the nucleus, respectively.

While nuclei with non-zero spin are sensitive to the SD interactions, nuclei with larger atomic or mass numbers are more sensitive to the SI interactions. The nucleon scalar

* While X is a Majorana fermion, we omit “1/2” in the coefficients of the interactions due to the convention given in Ref. [22].

operators in Eq. 8 become proton and neutron density operators in the non-relativistic limit. Thus, the amplitude is proportional to Z or $A - Z$.

Earlier, we ignored the nucleus form factors. However, they are not negligible in practice. Let us consider the SI cross section. The momentum transfer $q = |\vec{q}|$ is given by $(2m_T E_R)^{1/2}$, where the recoil energy E_R is $E_{th} \leq E_R \leq 2(m_r^2/m_T)v^2$. The nuclear radius r_N is typically $A^{1/3}$ fm, and then, $r_N q \simeq 7 \times 10^{-3} A^{5/6} (E_R(\text{keV}))^{1/2}$. While the SI cross sections are larger for larger nuclei, the SI cross sections suffer from suppression for large E_R and/or large A due to the form factors. Furthermore, the form factors are important to predict the precise spectrum of the nucleus recoil energy in direct detection. The nucleus form factors are reviewed in Ref. [23].

4 Brief Review of Direct Detection Experiments

The DM energy density around the earth is determined by the stellar motions in our galaxy. However, due to our limited knowledge of the DM density distribution in our galaxy, the energy distribution is still evaluated with a large uncertainty as [24]

$$\rho_X = (0.2 - 0.6) \text{GeV/cm}^3. \quad (11)$$

The DM velocity distribution is more uncertain since we have no way to measure it directly. A Maxwellian distribution $f(\vec{v})$ is assumed in the galactic center coordinate [23],

$$f(\vec{v}) \simeq \frac{1}{(\pi v_0^2)^{3/2}} e^{-(\vec{v} + \vec{v}_\oplus)^2/v_0^2}, \quad (12)$$

where $v_0 \simeq 230 \text{km/sec}$ and \vec{v}_\oplus is the Earth's velocity. This distribution is supported by the N -body simulations. The Earth's velocity is

$$|\vec{v}_\oplus| \simeq 244 + 15 \sin(2\pi y) \text{ (km/sec)}, \quad (13)$$

with y the elapsed time from March 2nd. The first term comes from the motion of the Solar System, and the second is from revolution of the Earth around the Sun. If WIMP wind relative to the Earth is detected by direction-sensitive detectors, it would be strong evidence for the DM, although it would still not be conclusive. Annual modulation of the event rate is also expected, and it is at most 3%.

Thus, the signals in the direct detection experiments are only from recoiled nuclei. The signals are observed by detecting phonons/heat, ionization, or light generated by the recoiled nuclei in the experiments. They have to maintain a low background in the experiments. The dominant backgrounds are gamma rays and electrons from the beta and gamma decays. The experiments are performed underground, and the coincidence of the signals, such as ionization and light in the XENON [19] and PandaX experiments [20], are observed.

The event rate per unit mass of the target R is given as

$$dR = \frac{N_0}{A} \sigma v \, dn_X, \quad (14)$$

(N_0 is the Avogadro number). Assuming a zero-momentum transfer cross section $\sigma \simeq \text{const} = \sigma_0$, the event rate is evaluated as

$$\begin{aligned} R_0 &= \frac{2}{\pi} \frac{N_0}{A} \frac{\rho_X}{M_X} \sigma_0 v_0 \\ &\simeq \frac{540}{AM_X} \left(\frac{\sigma_0}{10^{-36} \text{cm}^2} \right) \left(\frac{\rho_0}{0.4 \text{GeV/cm}^3} \right) \left(\frac{v_0}{230 \text{km/sec}} \right) \text{ event/kg/day}, \end{aligned} \quad (15)$$

where M_X is in GeV.

The event spectrum as a function of the recoil energy E_R is approximately given by [23]

$$\frac{dR}{dE_R} \simeq \frac{R_0}{E_0} e^{-E_R/E_0} \quad (16)$$

where $E_0 = 2(m_r^2/M_T)v^2$. Thus, if the energy threshold in the experiment is lowered, the event rate is increased and the experiments are more sensitive to WIMPs with lighter masses.

As explained in the previous section, the SI cross section of WIMPs with nuclei is enhanced when the target nucleus has large atomic or mass numbers. Thus, many experiments use heavy nuclei as the targets. If the SI interaction is isosinglet, the zero-momentum transfer SI cross sections with nuclei are proportional to the SI cross section with the proton σ_{SI}^p as

$$\sigma_0 = A^2 \frac{m_r^2(A)}{m_r^2(1)} \sigma_{\text{SI}}^p \quad (17)$$

with $m_r^2(A)$ ($m_r^2(1)$) the reduced mass of the target nucleus (proton) and the WIMP. The sensitivity and exclusion curves of the direct detection experiments are shown on a plane of σ_{SI}^p and M_X .

The current limits on the SI cross section of proton are derived from LUX [25], XENON1T [19], and PandaX-II [20]. They exclude up to $\sigma_{\text{SI}}^p \sim 10^{-46} \text{cm}^2$ for $M_X \simeq 50 \text{ GeV}$. The limits for heavier WIMPs are scaled by $1/M_X$ since the DM number density is ρ_X/M_X . The second-generation experiments, XENONnT, LZ, and PandaX-xT, whose fiducial volumes are $O(1)$ ton, will start in a few years [2]. These experiments will aim for 10^{-48} cm^2 .

Neutrino coherent scattering off nuclei is a serious background source in direct detection experiments, called “the neutrino floor” [26]. It is quite difficult to remove it except in direct detection experiments with directional sensitivity. The solar neutrinos hide the signals for light DM ($M_X \lesssim O(1) \text{ GeV}$) if $\sigma_{\text{SI}}^p \lesssim 10^{-44} \text{cm}^2$. The atmospheric neutrinos also hide the heavier DM signals if $\sigma_{\text{SI}}^p \lesssim 10^{-49} (10^{-48}) \text{cm}^2$ for $M_X \simeq 100 \text{ GeV}$ (1 TeV). The third-generation experiments aim to reach the neutrino floor [2].

5 Evaluation of Effective Interaction of WIMPs with Nucleons

We now evaluate the effective interactions of WIMPs with nucleons from UV theories. For this purpose, we first construct effective theories of WIMPs and quarks/gluons for direct detection experiments. The Wilson coefficients $C_i(\mu_{\text{UV}})$ ($i = 1, 2, \dots$) of the effective operators $O_i(\mu_{\text{UV}})$ at the UV scale μ_{UV} are derived by integrating out heavy particles in the UV theory. In the normal procedure for hadronic observables in flavor physics, the Wilson coefficients at the hadronic scale $\mu_H \sim 1$ GeV are derived from those at the UV scale using the RG equations. This is the case where our knowledge about the matrix elements of the effective operators is limited to those at the hadronic scale. However, some matrix elements relevant to DM direct detection are available at any μ so that we do not need to evaluate the Wilson coefficients at the hadronic scale ourselves, especially at the leading order of α_s .

In this section, we assume that the WIMPs are Majorana fermions, though the derivation in this section is applicable to the scalar and vector WIMPs, as given in Ref. [3].

5.1 Effective Theories at the Parton Level

When the WIMPs are Majorana fermions, the parton-level effective interactions relevant to DM direct detection at the hadronic scale are the following:

$$L_{\text{eff}} = \sum_{p=q,g} C_S^p O_S^p + \sum_{i=1,2} \sum_{p=q,g} C_{T_i}^p O_{T_i}^p + \sum_q C_{AV}^q O_{AV}^q , \quad (18)$$

with

$$\begin{aligned} O_S^q &\equiv \bar{X} X m_q \bar{q} q , \\ O_S^g &\equiv \bar{X} X \frac{\alpha_s}{\pi} G_{\mu\nu}^A G^{A\mu\nu} , \\ O_{T_1}^p &\equiv \frac{1}{M_X} \bar{X} i \partial^\mu \gamma^\nu X O_{\mu\nu}^p , \\ O_{T_2}^p &\equiv \frac{1}{M_X^2} \bar{X} i \partial^\mu i \partial^\nu X O_{\mu\nu}^p , \\ O_{AV}^q &\equiv \bar{X} \gamma_\mu \gamma_5 X \bar{q} \gamma^\mu \gamma_5 q , \end{aligned} \quad (19)$$

up to the equations of motions and the integration by parts. Here, q and $G_{\mu\nu}^A$ denote the light quarks ($q = u, d, s$) and the field strength tensor of the gluon field, respectively; m_q are the masses of the quarks; $\alpha_s \equiv g_s^2/(4\pi)$ is the strong coupling constant, $O_{\mu\nu}^q$ and $O_{\mu\nu}^g$ are called the spin-2 twist-2 operators of the quarks and the gluon, respectively,

$$\begin{aligned} O_{\mu\nu}^q &\equiv \frac{1}{2} \bar{q} i \left(D_\mu \gamma_\nu + D_\nu \gamma_\mu - \frac{1}{2} g_{\mu\nu} \not{D} \right) q , \\ O_{\mu\nu}^g &\equiv G_\mu^{A\rho} G_\nu^A - \frac{1}{4} g_{\mu\nu} G_{\rho\sigma}^A G^{A\rho\sigma} , \end{aligned} \quad (20)$$

with D_μ as the covariant derivatives. The quark or gluon field strength bilinear operators are up to dimension 4 in Eq. 18. The operators O_{AV}^q contribute to the SD interactions, while the other operators contribute to the SI ones.

The quark/gluon scalar operators in O_S^q and O_S^g are multiplied by m_q and α_s/π , respectively. The reasons are the following. The quark scalar operators are chiral symmetry-breaking so that they are multiplied by m_q . The nucleon matrix elements of $G_{\mu\nu}^A G^{A\mu\nu}$ are multiplied by π/α_s , compared with those of $m_q \bar{q}q$, as will be shown. This leads to a change in the power counting of α_s in the perturbation when evaluating the DM direct detection rate. Then, we multiply O_S^g by α_s/π . In addition, O_S^q and O_S^g are RG invariant at all orders and at the one-loop level, respectively, in QCD. These will be explained in next subsection in more detail.

Twist is defined as the mass dimension minus the spin of the operators. Higher spin or higher twist operators have more mass dimensions than the spin-2 twist-2 operators so they are negligible in DM direct detection [22]. The operators in O_{T1}^p and O_{T2}^p ($p = q, g$) have mass dimensions 8 and 9, respectively, higher than the others in Eq. 19. However, in the non-relativistic limit for WIMPs, $O_{T1}^p \simeq X^\dagger X O_{00}^p$ and $O_{T2}^p \simeq \bar{X} X O_{00}^p$, which behave as dimension-7 operators, since the operators in O_{T1}^p and O_{T2}^p are multiplied by $1/M_X$ and $1/M_X^2$, respectively[†] [22]. Unless the mediator particles generating those operators have masses much larger than M_X , the Wilson coefficients for O_{T1}^p and O_{T2}^p are not suppressed. Thus, they may contribute to the SI interactions, comparable to O_S^q and O_S^g .

5.2 Matrix Elements and RG Equations for Scalar Operators

First, let us discuss the nucleon matrix elements for the quark/gluon scalar operators. The matrix elements for the quark scalar operators in O_S^q are given by

$$\langle N | m_q \bar{q}q | N \rangle \equiv f_{T_q}^{(N)} m_N, \quad (21)$$

with $f_{T_q}^{(N)}$ the mass fraction parameters of the quark q . Presently, the mass fraction parameters of quarks are evaluated with lattice QCD simulations. The following were derived by the ETM collaboration with $N_f = 2 + 1 + 1$ [28],

$$\begin{aligned} f_{T_u}^p &= 0.0149(17)_{(16)}^{(21)}, & f_{T_u}^n &= 0.0117(15)_{(12)}^{(18)}, \\ f_{T_d}^p &= 0.0234(23)_{(16)}^{(27)}, & f_{T_d}^n &= 0.0298(23)_{(16)}^{(30)}, \\ f_{T_s}^N &= 0.0440(88)_{(15)}^{(72)}, \\ f_{T_c}^N &= 0.085(22)_{(7)}^{(11)}, \end{aligned} \quad (22)$$

($N = p, n$). The first and second parentheses are for statistical and systematical uncertainties, respectively. Heavier quarks have larger mass fraction parameters. In the simulations, the mass fraction parameter of the charm quark is also evaluated. We will return to this later.

[†] This is more transparent in heavy particle effective theories, where the WIMPs are treated as non-relativistic fields [27].

The nucleon matrix element of the gluon scalar operator is evaluated with the trace anomaly in QCD. The trace anomaly in QCD is [29]

$$\theta_\mu^\mu = \frac{\beta(\alpha_s)}{4\alpha_s} G_{\mu\nu}^A G^{A\mu\nu} + (1 - \gamma_m(\alpha_s)) \sum_q m_q \bar{q}q. \quad (23)$$

The beta function of α_s , $\beta(\alpha_s)$, and anomalous dimension of the quark mass, $\gamma_m(\alpha_s)$, are given by

$$\begin{aligned} \beta(\alpha_s) &\equiv \mu \frac{\partial}{\partial \mu} \alpha_s \simeq 2b_1 \frac{\alpha_s^2}{4\pi} + 2b_2 \frac{\alpha_s^3}{(4\pi)^2}, \\ \gamma_m(\alpha_s) m_q &\equiv \mu \frac{\partial}{\partial \mu} m_q \simeq -6C_F \frac{\alpha_s}{4\pi}, \end{aligned} \quad (24)$$

where $b_1 = -11N_c/3 + 2N_f/3$ and $b_2 = -34N_c^2/3 + 10N_cN_f/3 + 2C_FN_f$ ($N_c = 3$ and $C_F = 4/3$). The nucleon mass is given by the nucleon matrix element of the trace anomaly,

$$m_N \equiv \langle N | \theta_\mu^\mu | N \rangle. \quad (25)$$

Thus, the nucleon matrix element of the gluon scalar operator is given by

$$\begin{aligned} \langle N | \frac{\alpha_s}{\pi} G_{\mu\nu}^A G^{A\mu\nu} | N \rangle &= m_N \frac{4\alpha_s^2}{\pi\beta(\alpha_s)} \left[1 - (1 - \gamma_m(\alpha_s)) \sum_q f_{T_q}^{(N)} \right] \\ &\simeq -\frac{8}{9} m_N (1 - \sum_q f_{T_q}^{(N)}) + O(\alpha_s). \end{aligned} \quad (26)$$

We take $N_f = 3$ in the last of the above equations. When the gluon scalar operator is multiplied by α_s/π , the nucleon matrix element is $O(1)$ in units of m_N .

In most UV models, the WIMPs do not directly couple with gluons, and the effective interactions of the WIMPs with the gluon are generated by the integration of the quarks or other colored particles. This implies that the effective interaction for the gluon scalar operator is suppressed by α_s/π compared to those for the quark scalar operators. However, the nucleon matrix elements for the gluon scalar operators are $O(1)$ even if the gluon scalar operator is multiplied by α_s/π . Thus, we have to evaluate the higher-order contributions to the gluon scalar operator by α_s/π , in contrast to the quark scalar operators.

Let us discuss the contribution of the heavy quark scalar operators $m_Q \bar{Q}Q \bar{X}X$ to the gluon scalar operator in order to see the above counting of α_s . The nucleon matrix element of the trace anomaly is independent of the number of flavors N_f since it is a physical observable. This implies that

$$\begin{aligned} \langle N | m_Q \bar{Q}Q | N \rangle &= \frac{\pi \Delta\beta(\alpha_s)}{4(1 - \gamma_m(\alpha_s))\alpha_s^2} \langle N | \frac{\alpha_s}{\pi} G_{\mu\nu}^A G^{A\mu\nu} | N \rangle \\ &\simeq -\frac{1}{12} (1 + 11 \frac{\alpha_s}{4\pi}) \langle N | \frac{\alpha_s}{\pi} G_{\mu\nu}^A G^{A\mu\nu} | N \rangle \\ &\simeq \frac{2}{27} m_N, \end{aligned} \quad (27)$$

at $\mu \simeq m_Q$. Here, $\Delta\beta(\alpha_s) = \beta(\alpha_s)|_{N_f} - \beta(\alpha_s)|_{N_f-1}$. Thus, if the Wilson coefficients for the heavy and light quark scalar operators are common, the heavy quark contribution via the gluon scalar operator dominates over the light quark ones.

It is found that the numerical value in Eq. 27 is consistent with the mass fraction of the charm quark in Eq. 22. This coincidence is welcome, though a more precise determination of the mass fraction of the charm quark may reduce the uncertainty in the predicted direct detection rate. The charm quark mass is close to the hadronic scale so that the higher-dimensional operators might not be negligible after integrating out the charm quark. By integrating out the heavy quarks Q , the dimension-6 operators are generated as [30]

$$-\frac{\alpha_s}{12\pi}G_{\mu\nu}^AG^{A\mu\nu} + \frac{\alpha_s}{64\pi m_Q^2}(D^\nu G_{\nu\mu})^A(D_\rho G^{\rho\mu})^A - \frac{g_s\alpha_s}{720m_Q^2}f_{ABC}G_{\mu\nu}^AG^{\mu\rho B}G_{\rho}^{\nu C}. \quad (28)$$

The first term corresponds to the leading order term in the second line of Eq. 27. When $\Lambda_{\text{QCD}}^2/m_c^2 \simeq O(10)\%$, the coefficients of the higher-dimensional operators are numerically suppressed so that they are expected to be a few % of the leading term. This should be justified in lattice QCD in order to derive reliable predictions about the DM direct detection.

The anomalous dimensions of the scalar operators are also derived from the RG invariance of the quark scalar operators and the trace anomaly,

$$\mu \frac{\partial}{\partial \mu} m_q \bar{q}q = 0, \quad \mu \frac{\partial}{\partial \mu} \theta_\mu^\mu = 0. \quad (29)$$

It is found that

$$\mu \frac{\partial}{\partial \mu} (C_S^q, C_S^g) = (C_S^q, C_S^g) \Gamma_S, \quad (30)$$

where Γ_S is an $(N_f + 1) \times (N_f + 1)$ matrix,

$$\Gamma_S = \begin{pmatrix} 0 & \cdots & 0 & 0 \\ \vdots & \ddots & \vdots & \vdots \\ 0 & \cdots & 0 & 0 \\ -\frac{4\alpha_s^2}{\pi} \frac{\partial \gamma_m(\alpha_s)}{\partial \alpha_s} & \cdots & -\frac{4\alpha_s^2}{\pi} \frac{\partial \gamma_m(\alpha_s)}{\partial \alpha_s} & \alpha_s^2 \frac{\partial}{\partial \alpha_s} \left(\frac{\beta(\alpha_s)}{\alpha_s^2} \right) \end{pmatrix}. \quad (31)$$

C_S^q and C_S^g are RG-invariant in the leading term of $O(\alpha_s)$. The solutions for the above equations are

$$\begin{aligned} C_S^q(\mu) &= C_S^q(\mu_0) - \frac{4}{\pi} C_S^g(\mu_0) (\gamma_m(\alpha_s(\mu)) - \gamma_m(\alpha_s(\mu_0))), \\ C_S^g(\mu) &= \frac{\beta(\alpha_s(\mu))}{\alpha_s^2(\mu)} \frac{\alpha_s^2(\mu_0)}{\beta(\alpha_s(\mu_0))} C_S^g(\mu_0). \end{aligned} \quad (32)$$

5.3 Matrix Elements and RG Equations for Twist-2 Operators

Next are the matrix elements for the spin-2 twist-2 operators. The matrix elements are given by the parton-distribution functions (PDFs) of the nucleons ($N = p, n$) as

$$\begin{aligned}\langle N(p) | O_{\mu\nu}^q(\mu) | N(p) \rangle &= \frac{1}{m_N} \left(p_\mu p_\nu - \frac{1}{4} m_N^2 g_{\mu\nu} \right) (q^{(N)}(2; \mu) + \bar{q}^{(N)}(2; \mu)), \\ \langle N(p) | O_{\mu\nu}^g(\mu) | N(p) \rangle &= -\frac{1}{m_N} \left(p_\mu p_\nu - \frac{1}{4} m_N^2 g_{\mu\nu} \right) g^{(N)}(2; \mu),\end{aligned}\tag{33}$$

where $q^{(N)}(2; \mu)$, $\bar{q}^{(N)}(2; \mu)$, and $g^{(N)}(2; \mu)$ are the second moments of the PDFs for the quark, antiquark, and gluon, respectively. The n -th moments of the PDFs are defined as

$$\begin{aligned}q^{(N)}(n; \mu) &\equiv \int_0^1 dx x^{n-1} q^{(N)}(x; \mu), \\ \bar{q}^{(N)}(n; \mu) &\equiv \int_0^1 dx x^{n-1} \bar{q}^{(N)}(x; \mu), \\ g^{(N)}(n; \mu) &\equiv \int_0^1 dx x^{n-1} g^{(N)}(x; \mu),\end{aligned}\tag{34}$$

where $q^{(N)}(x; \mu)$, $\bar{q}^{(N)}(x; \mu)$, and $g^{(N)}(x; \mu)$ are the PDFs of the quark, antiquark, and gluon, respectively, at the factorization scale μ .

The derivation of Eq. 33 is given in standard textbooks of quantum field theory, such as texts by Peskin and Schroeder [31] or by Schwartz [32]. In the standard derivation, Operator Product Expansions (OPEs) are applied to Deeply-Inelastic Scattering (DIS), $e^- + N \rightarrow e^- + X$. In the expansion, the twist-2 operators are dominant, and the higher-twist operators are suppressed by the momentum transfer. From the contour integral of the OPEs on the complex plane of $\omega = 1/x$ (x : the Bjorken x in PDFs), it can be shown that

$$\langle N(p) | O_{\mu_1 \dots \mu_n}^q(\mu) | N(p) \rangle = \frac{1}{m_N} \{p^{\mu_1} \dots p^{\mu_n}\}_{\text{TS}} (q^{(N)}(n; \mu) + (-1)^n \bar{q}^{(N)}(n; \mu)),\tag{35}$$

where $O_{\mu_1 \dots \mu_n}^q(\mu)$ are twist-2 spin- n operators and “TS” means traceless symmetric. This derivation is for only the leading order term of Eq. 33. The μ dependence is introduced through the radiative correction. It can be shown that the anomalous dimensions for twist-2 operators are consistent with the Altarelli-Parisi evaluation of PDFs.

There is another derivation of Eq. 33. In the above derivation using DIS, it is assumed that the integral along $|\omega| \rightarrow \infty$ on the complex plane vanishes. If we define the PDFs using quantum fields, we may derive Eq. 33 in a rigorous way without such an assumption of a specific process. It has been proposed by Collins and Soper [33] that the PDFs be defined in light-cone coordinates. Eq. 33 is derived directly from the definition. Furthermore, Eq. 35 is the Mellin transformation of the PDFs in the mathematical language.

Thus, the inverse Mellin transformation of the matrix elements of twist-2 operators gives another definition of the PDFs. It gives a basis to evaluate of the PDFs in lattice QCD simulations [34].

Several groups evaluated the PDFs of partons by fitting with measurements in collider experiments, and they provide the PDFs at any factorization scale. The following are the second moments of the PDFs of proton derived by the CTEQ-Jefferson Lab. collaboration [35],

$$\begin{aligned}
g^{(p)}(2, \mu) &= 0.464(2), \\
u^{(p)}(2, \mu) &= 0.223(3), \quad \bar{u}^{(p)}(2, \mu) = 0.036(2), \\
d^{(p)}(2, \mu) &= 0.118(3), \quad \bar{d}^{(p)}(2, \mu) = 0.037(3), \\
s^{(p)}(2, \mu) &= 0.0258(4), \quad \bar{s}^{(p)}(2, \mu) = s(2, \mu), \\
c^{(p)}(2, \mu) &= 0.0187(2), \quad \bar{c}^{(p)}(2, \mu) = c(2, \mu), \\
b^{(p)}(2, \mu) &= 0.0117(1), \quad \bar{b}^{(p)}(2, \mu) = b(2, \mu),
\end{aligned} \tag{36}$$

where $\mu = m_Z$ and $N_f = 5$. The second moments of valence quarks and the gluon are $O(1)$ and those of the sea quarks are sub-leading, as expected. Those of the neutron are to be obtained by exchanging the values of the up and down quarks.

When using PDFs at a fixed factorization scale, we may need to evaluate the radiative correction between this scale and the UV scale. The anomalous dimensions of spin-2 twist-2 operators at the two-loop level are given by [37]

$$\mu \frac{d}{d\mu} (C_{T_i}^q, C_{T_i}^G) = (C_{T_i}^q, C_{T_i}^G) \Gamma_T, \tag{37}$$

with Γ_T an $(N_f + 1) \times (N_f + 1)$ matrix:

$$\Gamma_T = \begin{pmatrix} \gamma_{qq} & 0 & \cdots & 0 & \gamma_{qg} \\ 0 & \gamma_{qq} & & \vdots & \vdots \\ \vdots & & \ddots & 0 & \vdots \\ 0 & \cdots & 0 & \gamma_{qq} & \gamma_{qg} \\ \gamma_{gq} & \cdots & \cdots & \gamma_{gq} & \gamma_{gg} \end{pmatrix}, \tag{38}$$

where

$$\begin{aligned}
\gamma_{qq} &= \frac{16}{3} C_F \cdot \frac{\alpha_s}{4\pi} + \left(-\frac{208}{27} C_F N_f - \frac{224}{27} C_F^2 + \frac{752}{27} C_F N_c \right) \left(\frac{\alpha_s}{4\pi} \right)^2, \\
\gamma_{qg} &= \frac{4}{3} \cdot \frac{\alpha_s}{4\pi} + \left(\frac{148}{27} C_F + \frac{70}{27} N_c \right) \left(\frac{\alpha_s}{4\pi} \right)^2, \\
\gamma_{gq} &= \frac{16}{3} C_F \cdot \frac{\alpha_s}{4\pi} + \left(-\frac{208}{27} C_F N_f - \frac{224}{27} C_F^2 + \frac{752}{27} C_F N_c \right) \left(\frac{\alpha_s}{4\pi} \right)^2, \\
\gamma_{gg} &= \frac{4}{3} N_f \cdot \frac{\alpha_s}{4\pi} + \left(\frac{148}{27} C_F N_f + \frac{70}{27} N_c N_f \right) \left(\frac{\alpha_s}{4\pi} \right)^2.
\end{aligned} \tag{39}$$

5.4 Matrix Elements and RG Equations for Axial vector operators

The last one is the matrix elements of axial vector currents,

$$\langle N | \bar{q} \gamma_\mu \gamma_5 q | N \rangle \equiv 2S_\mu \Delta q_N, \quad (40)$$

where S_μ is for the nucleon spin and Δq_N is the spin fraction of quark q . The spin fractions of the quark are measured in DIS to be [36]

$$\begin{aligned} \Delta u_p &= 0.77, \\ \Delta d_p &= -0.47, \\ \Delta s_p &= -0.15. \end{aligned} \quad (41)$$

Those of the neutron are to be obtained by exchanging the values of the up and down quarks. The axial vector currents are RG invariant at the one-loop level.

5.5 Effective Interactions of WIMPs with Nucleons

The effective interactions of WIMPs with nucleons are evaluated using the nucleon matrix elements given in the previous subsection, as

$$\begin{aligned} f_N/m_N &= \sum_{q=u,d,s} C_s^q(\mu_H) f_{T_q}^{(N)} \\ &+ C_S^g(\mu_H) \frac{4\alpha_s^2(\mu_H)}{\pi\beta(\alpha_s(\mu_H))} \left(1 - (1 - \gamma_m(\mu_H)) \sum_{q=u,d,s} f_{T_q}^{(N)} \right) \\ &+ \frac{3}{4} \sum_{i=1,2} \sum_q^{N_f} C_{T_i}^q(\mu) (q(2; \mu) + \bar{q}(2; \mu)) - \frac{3}{4} \sum_{i=1,2} C_{T_i}^g(\mu) g(2; \mu), \end{aligned} \quad (42)$$

$$a_N = \sum_{q=u,d,s} C_{AV}^q(\mu_H) \Delta q. \quad (43)$$

As mentioned above, C_S^q , C_S^g , and C_{AV}^q are RG-invariant at the one-loop level. When calculating f_N and a_N at the leading order of α_s ,

$$\begin{aligned} C_S^q(\mu_H) &= C_S^q(\mu_{UV}), \quad (q = u, d, s), \\ C_S^g(\mu_H) &= C_S^g(\mu_{UV}) - \frac{1}{12} \sum_{q=c,b,t} C_S^q(\mu_{UV}), \\ C_{AV}^q(\mu_H) &= C_{AV}^q(\mu_{UV}), \quad (q = u, d, s). \end{aligned} \quad (44)$$

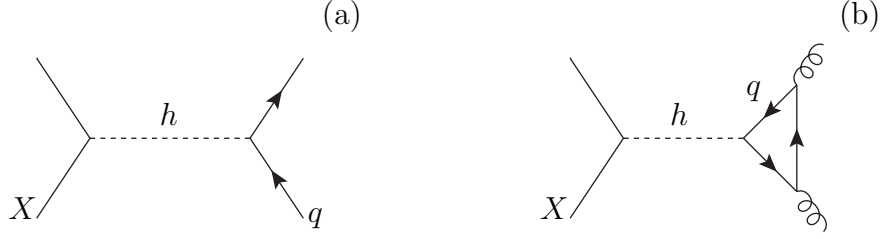


Figure 2: Diagrams for the effective couplings of singlet WIMPs induced by Higgs boson exchange at the parton level.

Thus, the scalar operator contribution to f_N is simplified as

$$\begin{aligned}
 f_N/m_N | \text{scalar op.} &= \sum_{q=u,d,s} C_S^q(\mu_{UV}) f_{T_q}^{(N)} \\
 &\quad - \frac{8}{9} (C_S^g(\mu_{UV}) - \frac{1}{12} \sum_{q=c,b,t} C_S^q(\mu_{UV})) \left(1 - \sum_{q=u,d,s} f_{T_q}^{(N)} \right).
 \end{aligned} \tag{45}$$

6 Examples (at Leading-Order of α_s)

We will now evaluate the effective interaction of WIMPs with the nucleon at the leading order of α_s , using the formulae in the previous section. We consider three models: 1) gauge-singlet WIMPs coupled with the Higgs boson, 2) gauge-singlet WIMPs coupled with colored scalars and quarks, and 3) $SU(2)_L$ non-singlet WIMPs. When the effective couplings of the WIMPs at the parton level are evaluated by integrating out heavy particles at the UV scale, we have to consider the case of matching the Wilson coefficients between the UV and effective theories.

6.1 Gauge Singlet WIMPs Coupled with Higgs Boson

We now consider a case where the WIMPs are $SU(2)_L$ singlet fermions X , coupled with the SM Higgs boson h as

$$L_{\text{int}} = -f_X \bar{X} X h. \tag{46}$$

This interaction is not symmetric under $SU(2)_L \times U(1)_Y$. However, this interaction is introduced in models where an $SU(2)_L$ singlet Higgs boson, coupled with X , is introduced, and it is mixed with the SM Higgs boson. Alternatively, such as in the SUSY SM, $SU(2)_L$ singlet and doublet fermions couple with the SM Higgs boson so that Eq. 46 is generated due to mixing of those fermions.

After integrating out the Higgs boson (Fig. 2), the quark scalar operators are generated as

$$C_S^q(\mu_{UV}) = \frac{1}{v_h m_h^2} f_X, \quad (47)$$

where v_h is the vacuum expectation value of the Higgs field ($v_H \simeq 246$ GeV) and m_h is the SM Higgs mass ($m_h \simeq 125$ GeV). The gluon scalar operator is generated by the integration of the heavy quarks, and the other operators are not generated at the leading order of α_s . Thus, the SI coupling constants with nucleons are given at the leading order of α_s by

$$f_N/m_N = \frac{1}{v_h m_h^2} f_X \left(\bar{f}_{T_q}^{(N)} + 3 \times \frac{2}{27} (1 - \bar{f}_{T_q}^{(N)}) \right), \quad (48)$$

where $\bar{f}_{T_q}^{(N)} \equiv \sum_{q=u,d,s} f_{T_q}^{(N)}$. From this result, the SI cross section of proton is $\sigma_{\text{SI}}^p \simeq 2 \times 10^{-42} \text{cm}^2 \times f_X^2$. The upperbound on σ_{SI}^p derived by XENON1T is about 10^{-46}cm^2 for $M_X \simeq 50$ GeV. Thus, $f_X \lesssim 10^{-2}$ for $M_X \simeq 50$ GeV.

6.2 Gauge Singlet WIMPs Coupled with Colored Scalars and Quarks

Next, we consider the case where colored scalars are introduced and the $\text{SU}(2)_L$ singlet WIMPs couple with the quarks and the colored scalars. Binos in the SUSY SM have such couplings with scalar quarks. Thus, this example corresponds to the limit of a heavy Higgsino in the SUSY SM, where the Bino–Higgs coupling is suppressed.

The interactions of WIMPs with quarks and colored scalars are given by

$$L_{\text{int}} = \sum_q \bar{q} (a_q + b_q \gamma_5) X \tilde{q} + \text{h.c.}, \quad (49)$$

where \tilde{q} is the colored scalar. The t -channel colored scalar exchange diagrams (Fig. 3) generate the quark scalar, twist-2, and axial vector operators, while the gluon scalar and twist-2 operators come from one-loop diagrams. Now, consider the leading contribution of α_s to the effective couplings of the WIMPs with nucleons. Thus, the one-loop contribution to the gluon scalar operator ((Fig. 4)) is included in the evaluation, while that to the gluon twist-2 operator is subleading, and is thus neglected.

From direct calculation, the Wilson coefficients for the quark operators are derived as

$$\begin{aligned} C_S^q(\mu_{UV}) &= \frac{a_q^2 - b_q^2}{4m_q} \frac{1}{M_X^2 - M_{\tilde{q}}^2} + \frac{a_q^2 + b_q^2}{8} \frac{M_X}{(M_X^2 - M_{\tilde{q}}^2)^2}, \\ C_{T1}^q(\mu_{UV}) &= \frac{a_q^2 + b_q^2}{2} \frac{M_X}{(M_X^2 - M_{\tilde{q}}^2)}, \\ C_{T2}^q(\mu_{UV}) &= 0, \\ C_{AV}^q(\mu_{UV}) &= -\frac{a_q^2 + b_q^2}{4} \frac{1}{M_X^2 - M_{\tilde{q}}^2}, \end{aligned} \quad (50)$$

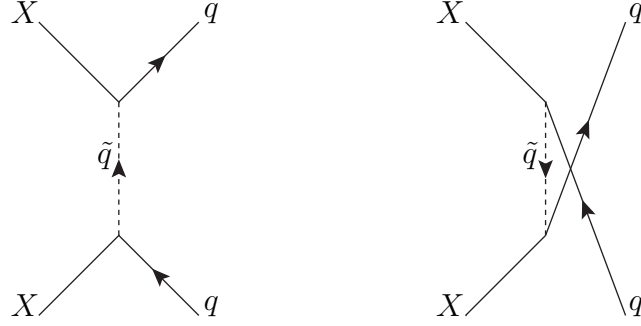


Figure 3: Diagrams for the effective couplings of singlet WIMPs with quarks induced by colored scalar exchange.

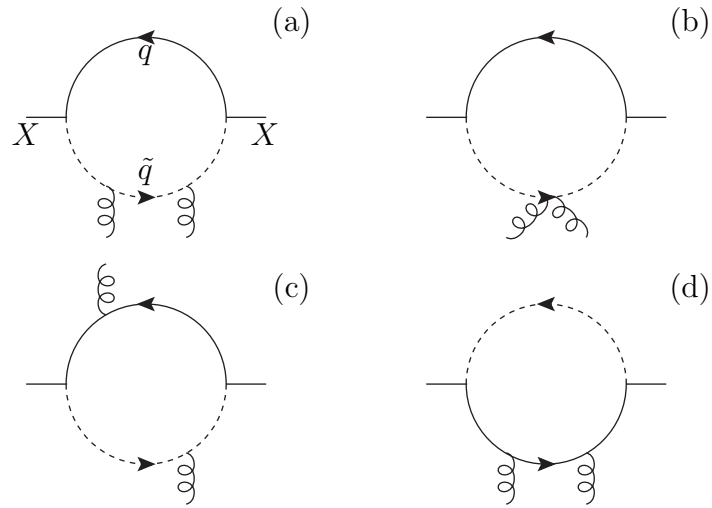


Figure 4: Diagrams for the effective couplings of singlet WIMPs with gluons induced by colored scalar exchange.

where $M_{\tilde{q}}$ is the colored scalar mass and $\mu_{UV} \simeq M_{\tilde{q}}$. The above Wilson coefficients are for quarks q with $m_q < \mu_{UV}$.

On the other hand, we have to match the UV and effective theories in order to derive the Wilson coefficient for the gluon scalar operator. The evaluation of the Wilson coefficients for operators including gluon field strengths is always troublesome due to the tensor structure. However, when the momenta of the external gluons are negligibly small and the gluon fields may be included as background fields, the Fock-Schwinger gauge ($x^\mu A_\mu^A(x) = 0$) is quite convenient for evaluating them, since we introduce propagators under the gluon field strength background with the gauge. Details of the technique are given in Appendix A.

Four one-loop diagrams in Fig. 4 contribute to the gluon scalar operator. While Diagrams *A* and *C* are automatically zero in the Fock-Schwinger gauge, Diagrams *B* and *D* give contributions to the gluon scalar operator as

$$\begin{aligned} C_S^g|_B &= \sum_q \left[\frac{a_q^2 + b_q^2}{16} \frac{M_X}{6M_{\tilde{q}}^2(M_X^2 - M_{\tilde{q}}^2)} \right], \\ C_S^g|_D &= \sum_q \left[-\frac{a_q^2 + b_q^2}{16} \frac{M_X}{6(M_X^2 - M_{\tilde{q}}^2)^2} - \frac{a_q^2 - b_q^2}{16} \frac{1}{3m_q M_{\tilde{q}}^2(M_X^2 - M_{\tilde{q}}^2)} \right]. \end{aligned} \quad (51)$$

Here, we take the leading terms of m_q assuming $m_q \ll M_{\tilde{q}}$ to demonstrate the matching. We find that $C_S^g|_D = -1/12 \sum_q C_S^q$. The contribution of Diagram *D* corresponds to the integration of heavy quarks in the effective theory. Thus,

$$C_S^g(\mu_{UV}) = \sum_{q=\text{all}} C_S^g|_D + \sum_{q(m_q > \mu_{UV})} C_S^g|_D. \quad (52)$$

In the above equations, the leading term of m_q is shown, though we should use the exact formulae when m_q is not negligible compared to M_X and $M_{\tilde{q}}$.

We can now show some numerical results. We assume that the singlet WIMPs have interactions with only the top and bottom quarks ($a_q = b_q = 0$ for $q = u, d, c, s$ and $a_q = b_q = 1/2$ for $q = t, b$). This is similar to the case where the binos are coupled with only the third-generation quarks and scalar quarks in the SUSY SM, assuming the other squarks are decoupled.

First, we should discuss the renormalization scale-dependence of the contribution from the twist-2 operators to the SI coupling constants of WIMPs with nucleons (the last two terms in Eq. 42). The Wilson coefficients for the quark/gluon scalar operators are RG invariant at the leading order of α_s , while those for the twist-2 operators are scale-dependent. As in Eq. 42, they may be evaluated at any scale if the factorization scale of the PDFs is properly chosen.

In the Fig. 5 the contribution from the twist-2 operators to the SI coupling constants of WIMPs with protons is shown, which is evaluated at $\mu = 2$ GeV and m_Z . The PDFs for $\mu = 2$ GeV and m_Z are also used. Here, we take $M_X = 200$ GeV and $M_{\tilde{q}} = 700$ GeV. The red and light-pink bars denote the uncertainties coming from the PDF input and

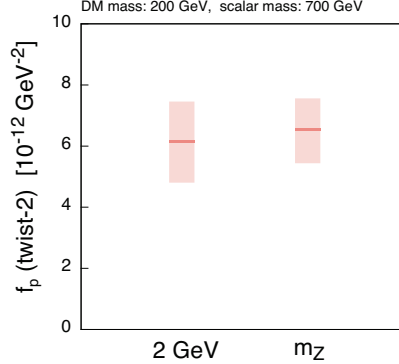


Figure 5: Contribution from twist-2 operators to the SI coupling constant of WIMPs with protons, evaluated at $\mu = 2 \text{ GeV}$ and m_Z . An explanation for the figure is given in the text. The figure comes from Ref. [3].

the perturbation in α_s , respectively. The method for evaluating the uncertainty from the PDFs' inputs is described in Ref. [35]. The uncertainty caused by neglecting the higher-order contributions in α_s is evaluated by varying the input and quark-mass threshold scales by a factor of two ($M_{\bar{q}}/2 \leq \mu \leq 2M_{\bar{q}}$, $m_t/2 \leq \mu \leq 2m_t$, and so on). The center values of the two calculations are almost the same, and the uncertainty from the perturbation in α_s for the case $\mu = 2 \text{ GeV}$ is slightly larger. This is expected from the nature of asymptotic freedom in QCD. Thus, it is better to evaluate the contribution from the twist-2 operators at the weak scale.

Next, the SI coupling constant (left) and the SI cross section of WIMPs with protons (right) as functions of the colored scalar mass are shown in Fig. 6. Here, $M_X = 200 \text{ GeV}$ again. In the left-hand figure, the upper (lower) solid line shows the contribution of the scalar-type (twist-2-type) operators to the SI coupling constant of WIMPs with protons. For the twist-2 contribution, we use PDFs at $\mu = m_Z$ and show the calculations both with and without the RG effects between $M_{\bar{q}}$ and m_Z in the solid and dashed lines, respectively. In the right-hand figure, the SI cross section of WIMPs with protons is shown with (solid) and without the RG effects (dashed line). The RG effects change the resulting value for the twist-2 contribution to the SI coupling constant by more than 50% when $M_{\bar{q}} = 500 \text{ GeV}$, and the scattering cross sections are modified by more than 20%. Thus, if the colored mediator mass is much larger than the factorization scale in the PDFs adopted in the evaluation, it is important to include the RG effects.

6.3 $\text{SU}(2)_L$ non-singlet WIMPs

Neutral components in the $\text{SU}(2)_L$ multiplets are candidates for WIMPs. If they are Dirac fermions or complex scalars with nonzero hypercharges, the DM direct detection experiments impose a strict bound on them. If the WIMP (X) is a fermion with hypercharge Y_X , the neutral current interaction induces SI interactions with nucleons ($N = n, p$) as

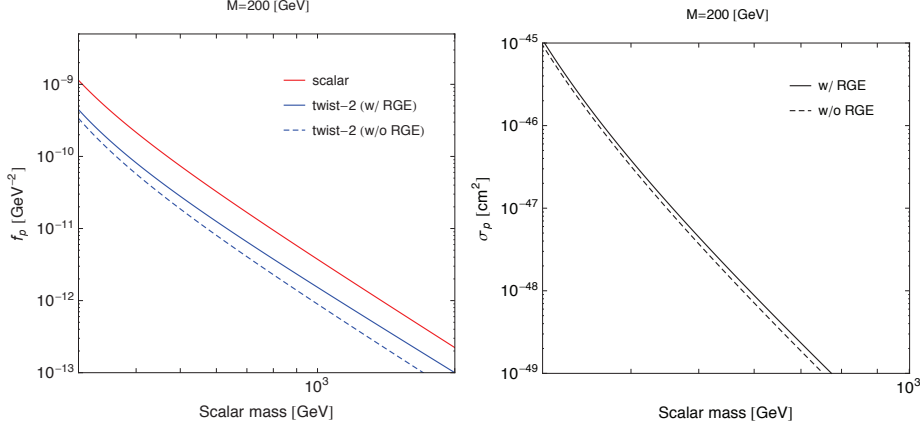


Figure 6: SI coupling constant (left) and SI cross section of WIMPs with protons (right) as functions of colored scalar mass. Here, $M_X = 200$ GeV. Explanation for figures is given in text. Figures come from Ref. [3].

follows,

$$L_{\text{eff}} = \sqrt{2}G_F Y_X \bar{X} \gamma_\mu X [(1 - 4 \sin^2 \theta_W) \bar{p} \gamma_\mu p - \bar{n} \gamma_\mu n] \quad (53)$$

where G_F and θ_W are the Fermi constant and Weinberg angle, respectively. The SI cross section of WIMPs with neutrons is larger than that with protons due to the accidental cancellation in the latter. They are insensitive to the WIMP mass, and the SI cross section with neutrons is approximately given by $Y_X^2 \times 7 \times 10^{-40} \text{cm}^2$. If the WIMPs are the dominant component of the DM in our galaxy, the mass should be larger than $\sim 10^5$ TeV. This is much heavier than the unitarity bound on the WIMP mass in the assumption that the WIMPs are in thermal equilibrium in the early universe [38]. Even if the WIMPs are complex scalars with nonzero hypercharge, a similar bound is derived. On the other hand, this constraint is avoidable if the WIMPs are Majorana fermions or real scalars, since their vector coupling is forbidden automatically.

$\text{SU}(2)_L$ triplet Majorana fermions with zero hypercharge are one of the examples. They are called winos in the SUSY SM, and they are superpartners of the weak gauge bosons. The triplet fermions include a neutral Majorana fermion and a charged Dirac fermion. The radiative corrections due to the $\text{SU}(2)_L$ gauge interactions generate the mass splitting between the neutral and charged fermions as $\Delta M_X \simeq 165$ MeV when $M_X \gg m_Z$ [39], and it makes the neutral fermion lighter than the charged one. The radiative corrections may easily dominate over the contribution to the mass splitting from effective operators induced by the integration of heavier particles, since the operators have mass dimensions of seven and above.

Now, assume that the triplet fermions have only gauge interactions.[‡] The WIMPs (the neutral component, X) only interact with the W boson and the charged component

[‡] In the SUSY SM, this situation is realized when the superpartners, except for gauginos, are decoupled such as in [40].

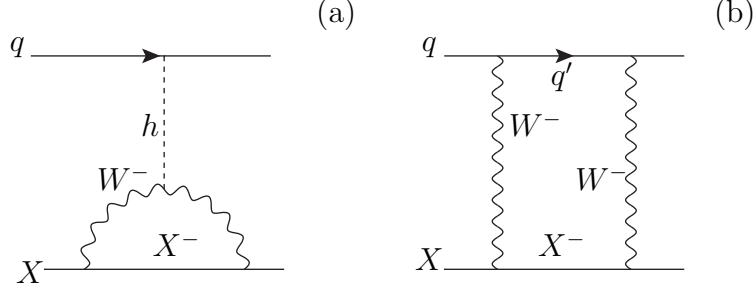


Figure 7: Diagrams for effective couplings of $SU(2)_L$ triplet fermion WIMPs with quarks.

X^- :

$$L_{int} = -g_2(\bar{X}\gamma^\mu X^- W_\mu^\dagger + \text{h.c.}). \quad (54)$$

In this case, the WIMPs couple with quarks at the one-loop level (Fig. 7), and with gluons at the two-loop level (Fig. 8). The diagrams give finite contributions, and the loop momenta in the diagrams are typically around m_W . Thus, we consider the effective theory with $N_f = 5$ flavors at $\mu_{UV} = m_Z$.

The Higgs boson exchange diagrams in Fig. 7 (a) and Fig. 8 (a) generate the scalar operators

$$\begin{aligned} C_S^q(\mu_{UV})|_{\text{Higgs}} &= \frac{\alpha_2^2}{4m_W m_h^2} g_H(\omega), \quad (q = u, d, s, c, b), \\ C_S^g(\mu_{UV})|_{\text{Higgs}} &= -\frac{\alpha_2^2}{48m_W m_h^2} g_H(\omega) \end{aligned} \quad (55)$$

where $\omega = m_W^2/M_X^2$ and $\alpha_2 = g_2^2/4\pi$. The coefficient $C_S^g(\mu_{UV})$ comes from the integration of the top quark. Here and in the following calculations, the mass difference between the charged and neutral fermions is neglected. The mass functions including $g_H(\omega)$ in this section are given in Ref. [4].

Next, let us calculate the contributions to the scalar operators from the box diagrams in Fig. 7 (b) and Fig. 8 (b) and (c). In this calculation, it is convenient to first derive the OPEs of the charged current-charged current correlator,

$$\Pi_{\mu\nu}^W(q) \equiv i \int d^4x \, e^{iqx} T \{ J_\mu^W(x) J_\nu^W(0)^\dagger \}, \quad (56)$$

where

$$J_\mu^W(x) = \sum_{i=1,2,3} \frac{g_2}{\sqrt{2}} \bar{u}_i \gamma_\mu P_L d_i. \quad (57)$$

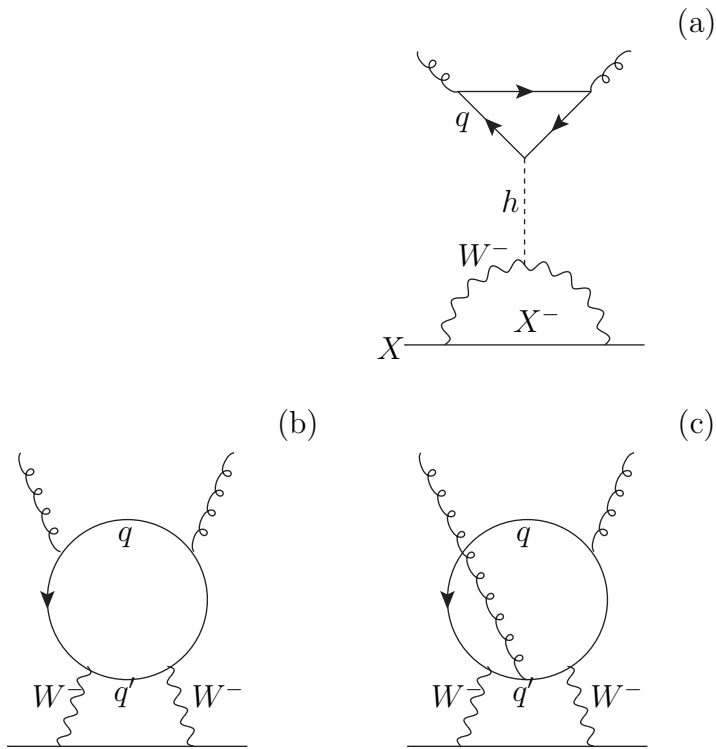


Figure 8: Diagrams for the effective couplings of $SU(2)_L$ triplet fermion WIMPs with gluons

The correlator is decomposed into its transverse $\Pi_T^W(q^2)$ and longitudinal parts $\Pi_L^W(q^2)$,

$$\Pi_{\mu\nu}^W(q) = ((-g_{\mu\nu} + \frac{q_\mu q_\nu}{q^2})\Pi_T^W(q^2) + \frac{q_\mu q_\nu}{q^2}\Pi_L^W(q^2)). \quad (58)$$

When connecting the correlator to the WIMP lines as in Fig. 7 (b) and Fig. 8 (b) and (c), the longitudinal part does not contribute to the scalar operators due to the gauge invariance [42].

The quark and gluon scalar operators in the transverse part of the correlator are represented by

$$\Pi_T^W(q)|_{\text{scalar}} = \sum_q^{N_f=5} c_{W,S}^q(q^2) m_q \bar{q}q + c_{W,S}^g(q^2) \frac{\alpha_s}{\pi} G_{\mu\nu}^A G^{A\mu\nu}. \quad (59)$$

The tree-level diagrams contribute to $c_{W,S}^q(q^2)$, though the $c_{W,S}^q(q^2)$ are suppressed by the tiny quark masses, since $J_\mu^W(x)$ is the $V-A$ current. The exception is $c_{W,S}^b(q^2)$,

$$c_{W,S}^b(q^2) = \frac{g_2^2 m_t^2}{8(q^2 - m_t^2)^2}, \quad (60)$$

due to the large top quark mass. On the other hand, the one-loop diagrams induce $c_{W,S}^g(q^2)$ as

$$c_{W,S}^g(q^2) = \frac{g_2^2}{48q^2} \left[2 + \frac{q^2}{q^2 - m_t^2} \right], \quad (61)$$

where the first and second terms in the bracket come from loop diagrams including the first two and third generations, respectively. Using these results, the Wilson coefficients for the scalar operator are

$$\begin{aligned} C_S^b(\mu_{UV})|_{\text{box}} &= \frac{\alpha_2^2}{m_W^3} [(-3)g_{\text{btm}}(\omega, \tau)], \\ C_S^g(\mu_{UV})|_{\text{box}} &= \frac{\alpha_2^2}{4m_W^3} [2g_{\text{B1}}(\omega) + g_{\text{top}}(\omega, \tau)] \end{aligned} \quad (62)$$

where $\tau = m_t^2/M_X^2$.

The contributions to the twist-2 operators also come from Fig. 7 (b) and Fig. 8 (b) and (c), though those to the gluon twist-2 operators are at $O(\alpha_s)$ so that they are neglected here. The OPEs in the charged current-charged current correlator involve the quark twist-2 operators at the leading order of α_s :

$$\begin{aligned} \Pi_{\mu\nu}^W &= \sum_{q=u,d,c,s} \frac{g_2^2}{2} \left[-\frac{g_{\mu\rho}g_{\nu\sigma}q^2 - g_{\mu\rho}q_\nu q_\sigma - q_\mu q_\rho g_{\nu\sigma} + g_{\mu\nu}q_\rho q_\sigma}{(q^2)^2} \right] O^{q\rho\sigma} \\ &+ \frac{g_2^2}{2} \left[-\frac{g_{\mu\rho}g_{\nu\sigma}(q^2 - m_t^2) - g_{\mu\rho}q_\nu q_\sigma - q_\mu q_\rho g_{\nu\sigma} + g_{\mu\nu}q_\rho q_\sigma}{(q^2 - m_t^2)^2} \right] O^{b\rho\sigma}. \end{aligned} \quad (63)$$

Then, the Wilson coefficients for the quark twist-2 operators are given by

$$\begin{aligned} C_{Ti}^q(\mu_{UV}) &= \frac{\alpha_2^2}{m_W^3} g_{Ti}(\omega, 0), \\ C_{Ti}^b(\mu_{UV}) &= \frac{\alpha_2^2}{m_W^3} g_{Ti}(\omega, \tau), \end{aligned} \quad (64)$$

($i = 1, 2$).

The axial vector coupling is also evaluated in a similar way:

$$C_{AV}^q = \frac{\alpha_2^2}{8m_W^2} g_{AV}(\omega). \quad (65)$$

We have now shown the Wilson coefficients at the leading order of α_s . Some of the Wilson coefficients are not suppressed even if M_X is much heavier than m_W . The Wilson coefficients for the gluon and scalar operators at the hadronic scale are

$$\begin{aligned} C_S^q(\mu_H) &\simeq \frac{\alpha_2^2}{4m_W m_h^2} (-2\pi), \\ C_S^g(\mu_H) &\simeq -3 \frac{\alpha_2^2}{48m_W m_h^2} (-2\pi) + 2 \frac{\alpha_2^2}{4m_W^3} \frac{\pi}{12} + \frac{\alpha_2^2}{4m_W^3} \frac{\pi}{24} \frac{3x_{tw} + 2}{(x_{tw} + 1)^3}, \end{aligned} \quad (66)$$

for $M_X \gg m_t, m_W$. Here, $x_{tw} = m_t/m_W$. The first term in $C_S^g(\mu_H)$ comes from the heavy quark contribution induced by the Higgs exchange, and the second and third are from box diagrams including the first two and third generations, respectively. The last one is more suppressed by the top quark mass compared to the box diagrams including light quarks. The Wilson coefficients for the quark twist-2 operators at μ_{UV} are

$$\begin{aligned} C_{T1}^q(\mu_{UV}) &= \frac{\alpha_2^2}{m_W^3} \frac{\pi}{3}, \\ C_{T2}^q(\mu_{UV}) &= O\left(\frac{m_W}{M_X}\right). \end{aligned} \quad (67)$$

The axial vector coupling constants are also suppressed by $O(m_W/M_X)$. Thus, the SI coupling constants become independent of M_X in the limit of $M_X \gg m_W$ while the SD coupling vanishes in the limit [42,43]. This implies that the SI cross sections are insensitive to the WIMP mass. This is welcome in the search for the WIMPs.

On the other hand, the contributions are comparable to each other so that the accidental cancellation suppresses the SI cross sections. The SI coupling constants of WIMPs with nucleons are roughly estimated as

$$f_N/m_N \simeq \frac{\alpha_2^2}{m_W^3} \times 0.4 - \frac{\alpha_2^2}{m_W^3} \times 0.27 - \frac{\alpha_2^2}{m_W^3} \times 0.03, \quad (68)$$

where the first, second, and third terms come from the quark twist-2 ($C_{T1}^q(\mu_{UV})$), gluon scalar ($C_S^g(\mu_H)$), and quark scalar operators ($C_S^q(\mu_H)$), respectively. This cancellation

reduces the SI cross sections by a factor of more than 10. In addition, it decreases the reliability of the calculation as the significance of the higher-order correction is relatively high [27]. The predicted SI cross sections are close to the neutrino SI scattering background, the neutrino floor. Thus, a more reliable evaluation method for the SI cross sections are needed.

The above calculation can be extended to the cases of $SU(2)_L$ n -plets [44]. Even if the hypercharge is nonzero, the WIMPs may be Majorana fermions or real scalars by introducing the effective coupling with the Higgs boson [45]. Higgsinos in the SUSY SM are $SU(2)_L$ doublets with hypercharges $\pm 1/2$, while the effective operator with the Higgs boson induced by integrating out gauginos decomposes a neutral Dirac fermion into two Majorana fermions with mass splitting.

7 Towards the Next-Leading Order Calculation of α_s

In the previous sections, we showed the evaluation of the elastic scattering cross section of WIMPs with nucleons at the leading order of α_s . In many phenomenological studies, the leading-order evaluation is enough, since the DM abundance around the earth still has large uncertainties. However, in some cases, evaluation at higher orders is required.

First, as in the case of $SU(2)_L$ triplet fermions, the accidental cancellation may suppress the leading order contribution. Many DM direct experiments are more sensitive to the SI cross section than the SD one. The SI cross section is induced from several contributions at the parton level, which interfere with each other. In the case of $SU(2)_L$ triplet fermions, the contributions to the SI coupling at the parton level are comparable to each other. Then, the destructive interference reduces the SI cross section significantly. The higher-order corrections have to be included in the evaluation of the SI cross section in order to be reliable.

Next is the uncertainty from the UV scale, μ_{UV} . The quark and gluon scalar operators are RG invariant at the leading order of α_s . Thus, their contribution is independent of μ_{UV} at the leading order. On the other hand, the SI cross section sensitive to the quark twist-2 operators at the leading order, and their Wilson coefficients depend on μ_{UV} . We need to include the next-leading order contribution in order to reduce the uncertainty from μ_{UV} .

Third, some next-leading order corrections are known to be large. For example, it is known that the threshold correction to the gluon scalar operator at the quark mass scale at the next-leading order is large.

The next-leading order evaluation of the elastic scattering cross section of WIMPs with nucleons is not yet complete. Some results for the SI cross section are shown in this section.

7.1 Matching Condition at Quark Mass Threshold

The Wilson coefficients for the quark and gluon scalar operators are not RG invariant at $O(\alpha_s^2)$. Thus, the two-loop RG equations for the Wilson coefficients need to be solved in order to derive $C_S^q(\mu_H)$ and $C_S^g(\mu_H)$ with μ_H the hadronic scale at the next-leading order of α_s . When the factorization scale of the PDFs, used in the evaluating the matrix elements of twist-2 operators, is different from the UV scale, we also include the correction of their two-loop RG equations. The RG equations for the Wilson coefficients are shown in Section 5.

At the heavy quark mass thresholds, we also have to include the threshold correction to the Wilson coefficients at $O(\alpha_s)$. When the bottom quark is decoupled and N_f is changed from 5 to 4, the matching conditions for the Wilson coefficients at the decoupling scale $\mu_b (\simeq m_b)$ are given by

$$\begin{aligned}
C_S^q(\mu_b)|_{N_f=4} &= C_S^q(\mu_b)|_{N_f=5}, \quad (q = u, d, s, c), \\
\alpha_s(\mu_b)C_S^g(\mu_b)|_{N_f=4} &= \left[1 + \frac{\alpha_s(\mu_b)}{4\pi} \frac{2}{3} \log \frac{m_b^2}{\mu_b^2}\right] \alpha_s(\mu_b)C_S^g(\mu_b)|_{N_f=5} \\
&\quad - \frac{\alpha_s(\mu_b)}{12} \left[1 + \frac{\alpha_s(\mu_b)}{4\pi} \left(11 + \frac{2}{3} \log \frac{m_b^2}{\mu_b^2}\right)\right] \alpha_s(\mu_b)C_S^b(\mu_b)|_{N_f=5}, \\
C_{Ti}^q(\mu_b)|_{N_f=4} &= C_{Ti}^q(\mu_b)|_{N_f=5}, \quad (i = 1, 2), \\
C_{Ti}^g(\mu_b)|_{N_f=4} &= \left[1 + \frac{\alpha_s(\mu_b)}{4\pi} \frac{2}{3} \log \frac{m_b^2}{\mu_b^2}\right] C_{Ti}^g(\mu_b)|_{N_f=5} \\
&\quad + \frac{\alpha_s(\mu_b)}{4\pi} \frac{2}{3} \log \frac{m_b^2}{\mu_b^2} C_{Ti}^b(\mu_b)|_{N_f=5}, \quad (i = 1, 2),
\end{aligned} \tag{69}$$

where

$$\frac{1}{\alpha_s(\mu_b)|_{N_f=4}} = \frac{1}{\alpha_s(\mu_b)|_{N_f=5}} + \frac{1}{(3\pi)} \log \frac{\mu_b}{m_b}. \tag{70}$$

These matching conditions are derived by comparing the two effective theories with $N_f = 5$ and 4. The logarithmic terms correspond to the RG equations. The large factor of 11 in the matching condition for C_S^g is found in the second line of Eq. 27. Thus, the threshold correction C_S^g at α_s is not negligible even if it is of the next-leading order [48].

Similar matching conditions are applied for the other heavy quark threshold. For example, the matching conditions for the twist-2 operators at μ_b are irrelevant to the practical calculation when the factorization scale of the PDFs is higher than μ_b . However, if μ_{UV} is higher than the top quark mass and the factorization scale is below the top quark mass, we have to include the radiative corrections between the two scales, taking account the top quark threshold. The matching conditions for C_{Ti}^g have to be included in the calculation.

7.2 Wilson Coefficients at UV Scale and SI Cross Sections at the Next-Leading Order of α_s

We now evaluate the SI cross section at the next-leading order of α_s . The calculation is very involved. We have to evaluate the Wilson coefficient $C_S^g(\mu_{UV})$ for the gluon scalar operator at higher orders of α_s than for the other operators in the UV theory. In the case of the Higgs portal singlet WIMPs, the calculation is the straightforward. For singlet WIMPs coupled with colored scalars and quarks, what we have to evaluate at the UV scale are the following:

Operators	LO	NLO
Quark scalar	tree	1 loop
Quark twist-2	tree	1 loop
Gluon scalar	1 loop	2 loop
Gluon twist-2.	—	1 loop

The coefficient for the gluon twist-2 operator from the one-loop diagrams is simultaneously calculated when calculating that of the gluon scalar operator at the leading order. However, the other contributions at the next-leading order have not yet been evaluated.

The last are the $SU(2)_L$ triplet fermions. When evaluating the SI cross sections for the $SU(2)_L$ triplet fermions at the next-leading order of α_s , we have to calculate the two and three-loop diagrams. This calculation cannot be done by hand, if we include all the next-leading order contributions. Fortunately, the quark and gluon scalar operators in the charged current-charged current correlator $\Pi_{\mu\nu}^W$ are evaluated at the three-loop level [46], and the twist-2 operators at the two-loop level [47], assuming the quarks are massless. In the leading order calculation, while the top quark mass is not negligible, the contributions of the third generation to the SI cross sections are suppressed by the top quark mass itself. Thus, we can neglect the next-leading order contributions of the third generation and evaluate the uncertainties from it.

In the Ref. [4], the following contributions are included in the evaluation of the Wilson coefficients at μ_{UV} with $N_f = 5$.

		Higgs		Box	
Paton	Orators	LO	NLO	LO	NLO
quark	scalar	1 loop	2 loop	-	2 loop
(1st and 2nd gen.)	twist-2	-	-	1 loop	2 loop
quark	scalar	1 loop	2 loop	1 loop	2 loop (neglected)
(bottom)	twist-2	-	-	1 loop	2 loop (neglected)
gluon	scalar	2 loop	3 loop	2 loop	3 loop
(1st and 2nd gen.)	twist-2	-	-	-	2 loop
gluon	scalar	2 loop	3 loop	2 loop	3 loop (neglected)
(3rd gen.)	twist-2	-	-	-	2 loop (neglected)

Here, “–” means that the contributions vanish. The column with “Higgs” is for the Higgs exchange diagrams and that with “box” is for box diagrams.

It is beyond the scope of this book to show the details of the calculation. The SI cross section in the limit of $M_X \gg m_W$ is found to be [4]

$$S_{rmSI}^p = 2.3_{-0.3-0.4}^{+0.2+0.5} \times 10^{-47} \text{cm}^2 \quad (71)$$

where the first error comes from perturbative uncertainties, mainly from the choice of μ_{UV} . The second one is from the input uncertainty, such as the PDFs. It is checked that neglecting the next-leading order contribution from the third generation quarks does not lead to significant errors. The SI cross section with protons is shown as a function of M_X in Fig. 9. The blue dashed and red solid lines represent the leading-order and next-leading order results, respectively, with corresponding bands for perturbative uncertainties. The gray band is for the uncertainty resulting from the input error. The yellow shaded area corresponds to the neutrino floor, where the neutrino background dominates the DM signal. Fortunately, the SI cross section in Eq. 71 is larger than the neutrino floor even if the WIMP mass is around the 3 TeV predicted from thermal production.

The above calculation is applicable to other $SU(2)_L$ multiplets [4]. If the WIMPs come from $SU(2)_L$ doublet fermions (Higgsinos in the SUSY SM), the SI cross section with protons is around 10^{-49}cm^2 , which is below the neutrino floor. On the other hand, larger $SU(2)_L$ multiplets predict larger SI cross sections. For example, $SU(2)_L$ quintuplet fermions with zero hypercharge predict $\sigma_{SI}^p \simeq 2 \times 10^{-46} \text{cm}^2$.

8 Summary

The DM direct detection experiments are important for tests of the WIMP DM, and they are a window to new physics at the TeV scale. The first-generation experiments, LUX, XENON1T, and PandaX-II, are giving the strict bounds on the SI cross sections of WIMPs with nucleons. In a few years, the second-generation experiments will begin,

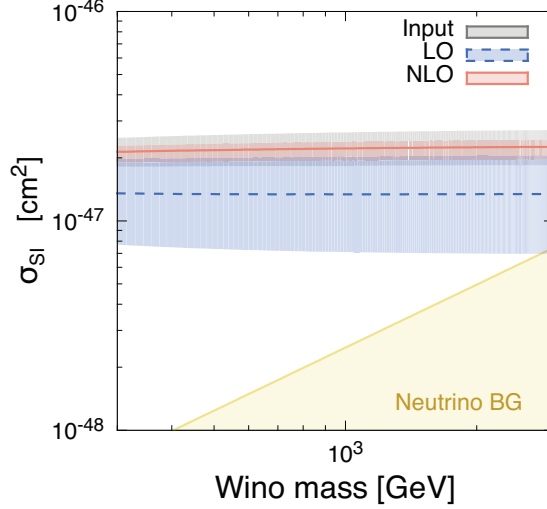


Figure 9: SI cross section of $SU(2)_L$ triplet fermions with nucleons. The (blue) dashed and (red) solid lines are for the leading-order and next-leading order results, respectively, with corresponding bands for perturbative uncertainties. The gray band is for uncertainty from input errors. In the yellow-shaded area the neutrino floor dominates the DM signals. Figure comes from Ref. [4].

LZ, XENONnT, and PandaX-nT with fiducial volumes $O(1)$ ton. The third-generation experiments with fiducial volumes $O(10)$ ton are also being planned in order to reach the neutrino floor. Thus, the theoretical predictions for the detection rates have to be more accurate and reliable in order to clarify their coverage to survey for WIMP models and their parameters.

In this lecture, the DM direct detection rates are evaluated with the effective theories. The effective theory approach is quite useful to evaluate them in a systematic way. We noted the QCD aspects in the evaluation of the effective coupling constants of WIMPs with nucleons. It is found that they are well controllable, and we may evaluate them at the next-leading order of α_s in the effective theory approach.

A Fock–Schwinger Gauge

The Fock–Schwinger gauge is convenient when evaluating the Wilson coefficients for the effective operators with $SU(3)_C$ field strengths. In the Feynman gauge, for example, it is tedious to maintain the tensor structure of the field strength. On the other hand, when using the Fock–Schwinger gauge, we may introduce the propagators of colored particles in the background of the gluon field strength, or the derivatives. Thus, we may maintain the tensor structure automatically. This review is based on Ref. [49].

The Fock–Schwinger gauge is given by

$$x^\mu A_\mu^A(x) = 0 \quad (72)$$

While this gauge fixing is not invariant under translation, the gauge field can be expanded at $x \simeq 0$ as

$$\begin{aligned} A_\mu^A(x) = & \frac{1}{2 \cdot 0!} x^\rho G_{\rho\mu}^A(0) + \frac{1}{3 \cdot 1!} x^\alpha x^\rho (D_\alpha G_{\rho\mu}(0))^A \\ & + \frac{1}{4 \cdot 2!} x^\alpha x^\beta x^\rho (D_\alpha D_\beta G_{\rho\mu}(0))^A + \dots \end{aligned} \quad (73)$$

The right-hand side in Eq. 73 is given with the gauge covariant terms, such as the gluon field strength or its derivatives.

For the proof, we first need the following relation in the Fock–Schwinger gauge,

$$A_\mu^A(x) = \int_0^1 d\alpha G_{\rho\mu}^A(\alpha x) \alpha x^\rho. \quad (74)$$

It is derived as follows. Using the gauge fixing condition, it is found that

$$A_\mu^A(y) = -y^\rho \frac{\partial A_\rho^A(y)}{\partial y^\mu} = y^\rho G_{\rho\mu}^A(y) - y^\rho \frac{\partial A_\mu^A(y)}{\partial y^\rho}. \quad (75)$$

By moving the second term in the right-hand side to the left-hand side, and taking $y = \alpha x$, we get

$$\begin{aligned} \alpha x^\rho G_{\rho\mu}^A(\alpha x) &= A_\mu^A(\alpha x) + x^\rho \frac{\partial A_\mu^A}{\partial x^\rho} \\ &= \frac{d}{d\alpha} (\alpha A_\mu^A(\alpha x)). \end{aligned} \quad (76)$$

Thus, Eq. 74 is derived.

Next, by expanding the gauge fixing condition at $x \simeq 0$ as

$$x^\mu (A_\mu^A(0) + x_{\alpha_1} \partial^{\alpha_1} A_\mu^A(0) + \frac{1}{2} x_{\alpha_1} x_{\alpha_2} \partial^{\alpha_1} \partial^{\alpha_2} A_\mu^A(0) + \dots) = 0, \quad (77)$$

we get

$$\begin{aligned} x^\mu A_\mu^A(0) &= 0, \\ x^\mu x_{\alpha_1} \partial^{\alpha_1} A_\mu^A(0) &= 0, \\ x^\mu x_{\alpha_1} x_{\alpha_2} \partial^{\alpha_1} \partial^{\alpha_2} A_\mu^A(0) &= 0, \\ \dots &= 0. \end{aligned} \quad (78)$$

Using these results, it is found that

$$x_{\alpha_1} \dots x_{\alpha_n} \partial^{\alpha_1} \dots \partial^{\alpha_n} G_{\rho\mu}^A(0) = x_{\alpha_1} \dots x_{\alpha_n} (D^{\alpha_1} \dots D^{\alpha_n} G_{\rho\mu}(0))^A. \quad (79)$$

By expanding Eq. 74 around $x \simeq 0$ and applying Eq. 79 to it, we get Eq. 73. In addition, using Eq. 78, the following equation for fermions (and also for scalars) is also derived,

$$\psi(x) = \psi(0) + x^\alpha D_\alpha \psi(0) + \frac{1}{2} x^\alpha x^\beta D_\alpha D_\beta \psi(0) + \dots \quad (80)$$

Next, we derive the quark propagator in the gluon field background, defined as

$$(i\partial_\mu \gamma^\mu - g_s \not{A} - m_q) iS(x, y) = i\delta^{(4)}(x - y), \quad (81)$$

where $\not{A} = A_\mu^A T_A \gamma_\mu$. The propagator is derived in a perturbative way as

$$\begin{aligned} iS(x, y) &= iS^{(0)}(x - y) + \int d^4 z iS^{(0)}(x - z) (-ig_s \not{A}(z)) iS^{(0)}(z - y) \\ &+ \int d^4 z d^4 z' iS^{(0)}(x - z) (-ig_s \not{A}(z)) iS^{(0)}(z - z') (-ig_s \not{A}(z')) iS^{(0)}(z' - y) \\ &+ \dots, \end{aligned} \quad (82)$$

where $iS^{(0)}(x - y)$ is the propagator under no gluon background. The gluon background field A_μ^A may be replaced with the gluon field strength or its covariant derivatives using Eq. 73 in the Fock–Schwinger gauge. In momentum space, A_μ^A is given by

$$\begin{aligned} A_\mu^A(k) &= \int d^4 x A_\mu^A(x) e^{ikx} \\ &= \frac{i}{2} (2\pi)^4 G_{\mu\rho}^A(0) \frac{\partial}{\partial k_\rho} \delta^{(4)}(k) \dots, \end{aligned} \quad (83)$$

where the covariant derivatives of $G_{\mu\rho}^A(0)$ are omitted here since they are irrelevant to the calculation of the DM detection rates in the text.

Using the above results, we get

$$\begin{aligned} iS(p) &= \int d^4 x e^{ipx} \langle T\{\psi(x) \bar{\psi}(0)\} \rangle \\ &= iS^{(0)}(p) \\ &+ \int d^4 k_1 iS^{(0)}(p) g_s \gamma^\alpha \left(\frac{1}{2} G_{\alpha\mu} \frac{\partial}{\partial k_{1\mu}} \delta^{(4)}(k_1) \right) iS^{(0)}(p - k_1) \\ &+ \int d^4 k_1 d^4 k_2 iS^{(0)}(p) g_s \gamma^\alpha \left(\frac{1}{2} G_{\alpha\mu} \frac{\partial}{\partial k_{1\mu}} \delta^{(4)}(k_1) \right) iS^{(0)}(p - k_1) g_s \gamma^\beta \\ &\times \left(\frac{1}{2} G_{\beta\nu} \frac{\partial}{\partial k_{2\nu}} \delta^{(4)}(k_2) \right) iS^{(0)}(p - k_1 - k_2) + \dots, \end{aligned} \quad (84)$$

where $iS^{(0)}(p) = i/(\not{p} - m_q)$ and $G_{\mu\nu} \equiv G_{\mu\nu}^A T_A$.

Since translation invariance is broken due to the gauge fixing, $S(0, x)$ does not have the same form as $S(x, 0)$,

$$\begin{aligned}
i\tilde{S}(p) &\equiv \int d^4x \, e^{-ipx} \langle T\{\psi(0)\bar{\psi}(x)\} \rangle \\
&= iS^{(0)}(p) \\
&+ \int d^4k_1 \, iS^{(0)}(p+k_1) \, g_s \gamma^\alpha \left(\frac{1}{2} G_{\alpha\mu} \frac{\partial}{\partial k_{1\mu}} \delta^{(4)}(p) \right) iS^{(0)}(p) \\
&+ \int d^4k_1 d^4k_2 \, iS^{(0)}(p+k_1+k_2) \, g_s \gamma^\alpha \left(\frac{1}{2} G_{\alpha\mu} \frac{\partial}{\partial k_{2\mu}} \delta^{(4)}(k_2) \right) \\
&\quad \times iS^{(0)}(p+k_1) \, g_s \gamma^\beta \left(\frac{1}{2} g G_{\beta\nu} \frac{\partial}{\partial k_{1\nu}} \delta^{(4)}(k_1) \right) iS^{(0)}(p) + \dots \quad (85)
\end{aligned}$$

The colored scalar propagator in the gluon background is also derived as

$$\begin{aligned}
i\Delta(p) &\equiv \int d^4x \, e^{ipx} \langle T\{\phi(x)\phi^\dagger(0)\} \rangle \\
&= i\Delta^{(0)}(p) \\
&+ \int d^4k_1 \, i\Delta^{(0)}(p) \, g_s(2p-k_1)^\alpha \left(\frac{1}{2} G_{\alpha\mu} \frac{\partial}{\partial k_{1\mu}} \delta^{(4)}(k_1) \right) i\Delta^{(0)}(p-k_1) \\
&+ \int d^4k_1 d^4k_2 \, i\Delta^{(0)}(p) \, g_s(2p-k_1)^\alpha \left(\frac{1}{2} G_{\alpha\mu} \frac{\partial}{\partial k_{1\mu}} \delta^{(4)}(k_1) \right) i\Delta^{(0)}(p-k_1) \\
&\quad \times g_s(2p-2k_1-k_2)^\beta \left(\frac{1}{2} G_{\beta\nu} \frac{\partial}{\partial k_{2\nu}} \delta^{(4)}(k_2) \right) i\Delta^{(0)}(p-k_1-k_2) \\
&+ \int d^4k_1 d^4k_2 \, i\Delta^{(0)}(p) (-ig_s^2) \left(\frac{1}{2} G_{\alpha\mu} \frac{\partial}{\partial k_{1\mu}} \delta^{(4)}(k_1) \right) \left(\frac{1}{2} G_{\nu}^\alpha \frac{\partial}{\partial k_{2\nu}} \delta^{(4)}(k_2) \right) \\
&\quad \times i\Delta^{(0)}(p-k_1-k_2) \, , \quad (86)
\end{aligned}$$

$$\begin{aligned}
i\tilde{\Delta}(p) &\equiv \int d^4x \, e^{-ipx} \langle T\{\phi(0)\phi^\dagger(x)\} \rangle \\
&= i\Delta^{(0)}(p) \\
&+ \int d^4k_1 \, i\Delta^{(0)}(p+k_1) \, g_s(2p+k_1)^\alpha \left(\frac{1}{2} G_{\alpha\mu} \frac{\partial}{\partial k_{1\mu}} \delta^{(4)}(k_1) \right) i\Delta^{(0)}(p) \\
&+ \int d^4k_1 d^4k_2 \, i\Delta^{(0)}(p+k_1+k_2) \, g_s(2p+2k_1+k_2)^\alpha \left(\frac{1}{2} G_{\alpha\mu} \frac{\partial}{\partial k_{1\mu}} \delta^{(4)}(k_2) \right) \\
&\quad \times i\Delta^{(0)}(p+k_1) \, g_s(2p+k_1)^\beta \left(\frac{1}{2} G_{\beta\nu} \frac{\partial}{\partial k_{2\nu}} \delta^{(4)}(k_1) \right) i\Delta^{(0)}(p) \\
&+ \int d^4k_1 d^4k_2 \, i\Delta^{(0)}(p+k_1+k_2) \\
&\quad \times (-ig_s^2) \left(\frac{1}{2} G_{\alpha\mu} \frac{\partial}{\partial k_{1\mu}} \delta^{(4)}(k_1) \right) \left(\frac{1}{2} G_{\nu}^\alpha \frac{\partial}{\partial k_{2\nu}} \delta^{(4)}(k_2) \right) i\Delta^{(0)}(p) \, , \quad (87)
\end{aligned}$$

where $i\Delta^{(0)}(p) = i/(p^2 - m^2)$. The scalar propagators are reduced to a more convenient form for practical usage as [50]

$$\begin{aligned}
i\Delta(p) &= i\Delta^{(0)}(p) \\
&+ \int d^4k_1 d^4k_2 i\Delta^{(0)}(p)(-ig_s^2) \left(\frac{1}{2} G_{\alpha\mu} \frac{\partial}{\partial k_{1\mu}} \delta^{(4)}(k_1) \right) \left(\frac{1}{2} G_{\nu}^{\alpha} \frac{\partial}{\partial k_{2\nu}} \delta^{(4)}(k_2) \right) \\
&\quad \times i\Delta^{(0)}(p - k_1 - k_2) \\
&\quad + \dots, \\
i\tilde{\Delta}(p) &= i\Delta^{(0)}(p) \\
&+ \int d^4k_1 d^4k_2 i\Delta^{(0)}(p + k_1 + k_2) \\
&\quad \times (-ig_s^2) \left(\frac{1}{2} G_{\alpha\mu} \frac{\partial}{\partial k_{1\mu}} \delta^{(4)}(k_1) \right) \left(\frac{1}{2} G_{\nu}^{\alpha} \frac{\partial}{\partial k_{2\nu}} \delta^{(4)}(k_2) \right) i\Delta^{(0)}(p) \\
&\quad \dots.
\end{aligned} \tag{88}$$

The scalar operator of the gluon $G_{\mu\nu}^A G^{A\mu\nu}$ is projected out from the bilinear term of the gluon field strength as

$$\begin{aligned}
G_{\alpha\mu}^A G_{\beta\nu}^A &= \frac{1}{12} G_{\rho\sigma}^A G^{A\rho\sigma} (g_{\alpha\beta} g_{\mu\nu} - g_{\alpha\nu} g_{\beta\mu}) \\
&- \frac{1}{2} g_{\alpha\beta} O_{\mu\nu}^g - \frac{1}{2} g_{\mu\nu} O_{\alpha\beta}^g - \frac{1}{2} g_{\alpha\nu} O_{\beta\mu}^g - \frac{1}{2} g_{\beta\mu} O_{\alpha\nu}^g \\
&+ O_{\alpha\mu\beta\nu}^g,
\end{aligned} \tag{89}$$

where $O_{\mu\nu}^g$ is the twist-2 operator of gluon (Eq. (20)) and $O_{\alpha\mu\beta\nu}^g$ is given as

$$\begin{aligned}
O_{\alpha\mu\beta\nu}^g &\equiv G_{\alpha\mu}^A G_{\beta\nu}^A \\
&- \frac{1}{2} g_{\alpha\beta} G_{\mu}^{A\rho} G_{\rho\nu}^A - \frac{1}{2} g_{\mu\nu} G_{\alpha}^{A\rho} G_{\rho\beta}^A + \frac{1}{2} g_{\alpha\nu} G_{\beta}^{A\rho} G_{\rho\mu}^A + \frac{1}{2} g_{\beta\mu} G_{\alpha}^{A\rho} G_{\rho\nu}^A \\
&+ \frac{1}{6} G_{\rho\sigma}^A G^{A\rho\sigma} (g_{\alpha\beta} g_{\mu\nu} - g_{\alpha\nu} g_{\beta\mu}).
\end{aligned} \tag{90}$$

Finally, we show Eq. 27 by integrating out heavy quarks in the Fock–Schwinger gauge. In the text, we derived this using the trace anomaly in QCD. Here, we will show it in a diagrammatic way. As in Fig. 10, two diagrams contribute there. However, in the Fock–Schwinger gauge, it is given by the trace of the quark propagator as

$$iM = -im_Q \int \frac{d^4p}{(4\pi)^4} \text{Tr}_{C+L} [iS(p)] = i \frac{\alpha_s}{12\pi} G_{\rho\sigma}^A G^{A\rho\sigma}. \tag{91}$$

While the Fock–Schwinger gauge is not invariant under translation, the invariance is recovered in the gauge-invariant results. The above calculation is quite easy compared with the other gauges, such as the Feynman gauge.

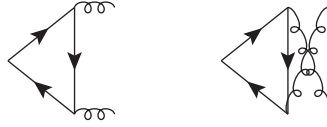


Figure 10: Integrating out the heavy quark.

References

- [1] For reviews of dark matter, G. Jungman, M. Kamionkowski and K. Griest, Phys. Rept. **267** (1996) 195 [hep-ph/9506380];
K. A. Olive, “TASI lectures on dark matter,” astro-ph/0301505;
G. Bertone, D. Hooper and J. Silk, Phys. Rept. **405** (2005) 279 [hep-ph/0404175];
J. L. Feng, Ann. Rev. Astron. Astrophys. **48** (2010) 495 [arXiv:1003.0904 [astro-ph.CO]].
- [2] T. Marrodn Undagoitia and L. Rauch, J. Phys. G **43** (2016) no.1, 013001 [arXiv:1509.08767 [physics.ins-det]].
- [3] J. Hisano, R. Nagai and N. Nagata, JHEP **1505** (2015) 037 [arXiv:1502.02244 [hep-ph]].
- [4] J. Hisano, K. Ishiwata and N. Nagata, JHEP **1506** (2015) 097 [arXiv:1504.00915 [hep-ph]].
- [5] P. A. R. Ade *et al.* [Planck Collaboration], Astron. Astrophys. (2014) [arXiv:1303.5076 [astro-ph.CO]].
- [6] For reviews of SUSY SM and SUSY DM, G. Jungman, M. Kamionkowski and K. Griest in [1];
S. P. Martin, Adv. Ser. Direct. High Energy Phys. **21** (2010) 1 [Adv. Ser. Direct. High Energy Phys. **18** (1998) 1] [hep-ph/9709356].
- [7] T. Appelquist, H. C. Cheng and B. A. Dobrescu, Phys. Rev. D **64** (2001) 035002 [hep-ph/0012100].
- [8] H. C. Cheng, J. L. Feng and K. T. Matchev, Phys. Rev. Lett. **89** (2002) 211301 [hep-ph/0207125];
H. C. Cheng, K. T. Matchev and M. Schmaltz, Phys. Rev. D **66** (2002) 036005 [hep-ph/0204342].
- [9] The Boltzmann equation for WIMPs is given in standard textbooks, such as E. W. Kolb and M. S. Turner, “The Early Universe.”
- [10] J. Edsjo and P. Gondolo, Phys. Rev. D **56** (1997) 1879 [hep-ph/9704361].

- [11] J. Hisano, S. Matsumoto, M. Nagai, O. Saito and M. Senami, Phys. Lett. B **646** (2007) 34 [hep-ph/0610249];
M. Cirelli, A. Strumia and M. Tamburini, Nucl. Phys. B **787** (2007) 152 [arXiv:0706.4071 [hep-ph]].
- [12] M. Ajello *et al.* [Fermi-LAT Collaboration], Astrophys. J. **819** (2016) no.1, 44 [arXiv:1511.02938 [astro-ph.HE]].
- [13] M. Ackermann *et al.* [Fermi-LAT Collaboration], Phys. Rev. Lett. **115** (2015) no.23, 231301 [arXiv:1503.02641 [astro-ph.HE]];
M. L. Ahnen *et al.* [MAGIC and Fermi-LAT Collaborations], JCAP **1602** (2016) no.02, 039 [arXiv:1601.06590 [astro-ph.HE]].
- [14] A. Abramowski *et al.* [H.E.S.S. Collaboration], Phys. Rev. Lett. **106** (2011) 161301 [arXiv:1103.3266 [astro-ph.HE]];
M. L. Ahnen *et al.* in [13].
- [15] M. Aguilar *et al.* [AMS Collaboration], Phys. Rev. Lett. **117** (2016) no.9, 091103.
- [16] M. G. Aartsen *et al.* [IceCube Collaboration], Phys. Rev. Lett. **110** (2013) no.13, 131302 [arXiv:1212.4097 [astro-ph.HE]].
- [17] K. Choi *et al.* [Super-Kamiokande Collaboration], Phys. Rev. Lett. **114** (2015) no.14, 141301 [arXiv:1503.04858 [hep-ex]].
- [18] J. Hisano, S. Matsumoto and M. M. Nojiri, Phys. Rev. Lett. **92** (2004) 031303 [hep-ph/0307216];
J. Hisano, S. Matsumoto, M. M. Nojiri and O. Saito, Phys. Rev. D **71** (2005) 063528 [hep-ph/0412403];
J. Hisano, S. Matsumoto, O. Saito and M. Senami, Phys. Rev. D **73** (2006) 055004 [hep-ph/0511118].
- [19] E. Aprile *et al.* [XENON Collaboration], Phys. Rev. Lett. **119** (2017) no.18, 181301 [arXiv:1705.06655 [astro-ph.CO]].
- [20] X. Cui *et al.* [PandaX-II Collaboration], Phys. Rev. Lett. **119** (2017) no.18, 181302 [arXiv:1708.06917 [astro-ph.CO]].
- [21] J. Fan, M. Reece and L. T. Wang, JCAP **1011** (2010) 042 [arXiv:1008.1591 [hep-ph]].
- [22] M. Drees and M. Nojiri, Phys. Rev. D **48** (1993) 3483 [hep-ph/9307208].
- [23] J. D. Lewin and P. F. Smith, Astropart. Phys. **6** (1996) 87.
- [24] J. I. Read, J. Phys. G **41** (2014) 063101 [arXiv:1404.1938 [astro-ph.GA]].
- [25] D. S. Akerib *et al.* [LUX Collaboration], Phys. Rev. Lett. **118** (2017) no.2, 021303 [arXiv:1608.07648 [astro-ph.CO]].

- [26] A. Gutlein *et al.*, Astropart. Phys. **34** (2010) 90 [arXiv:1003.5530 [hep-ph]];
J. Billard, L. Strigari and E. Figueroa-Feliciano, Phys. Rev. D **89** (2014) no.2, 023524 [arXiv:1307.5458 [hep-ph]];
F. Ruppin, J. Billard, E. Figueroa-Feliciano and L. Strigari, Phys. Rev. D **90** (2014) no.8, 083510 [arXiv:1408.3581 [hep-ph]].
- [27] R. J. Hill and M. P. Solon, Phys. Rev. Lett. **112** (2014) 211602 [arXiv:1309.4092 [hep-ph]].
- [28] A. Abdel-Rehim *et al.* [ETM Collaboration], Phys. Rev. Lett. **116** (2016) no.25, 252001 [arXiv:1601.01624 [hep-lat]].
- [29] M. A. Shifman, A. I. Vainshtein and V. I. Zakharov, Phys. Lett. **78B** (1978) 443.
- [30] L. Vecchi, [arXiv:1312.5695];
P. L. Cho and E. H. Simmons, Phys. Rev. D **51** (1995) 2360 [hep-ph/9408206].
- [31] M. E. Peskin and D. V. Schroeder, “An Introduction to quantum field theory.”
- [32] M. D. Schwartz, “Quantum Field Theory and the Standard Model.”
- [33] J. C. Collins and D. E. Soper, Nucl. Phys. B **194** (1982) 445.
- [34] D. E. Soper, Nucl. Phys. Proc. Suppl. **53** (1997) 69 [hep-lat/9609018].
- [35] J. F. Owens, A. Accardi and W. Melnitchouk, Phys. Rev. D **87** (2013) no.9, 094012 [arXiv:1212.1702 [hep-ph]].
- [36] D. Adams *et al.* [Spin Muon Collaboration], Phys. Lett. B **357** (1995) 248.
- [37] E. G. Floratos, D. A. Ross and C. T. Sachrajda, Nucl. Phys. B **152** (1979) 493;
A. Gonzalez-Arroyo and C. Lopez, Nucl. Phys. B **166** (1980) 429.
- [38] K. Griest and M. Kamionkowski, Phys. Rev. Lett. **64** (1990) 615.
- [39] M. Ibe, S. Matsumoto and R. Sato, Phys. Lett. B **721** (2013) 252 [arXiv:1212.5989 [hep-ph]].
- [40] L. Randall and R. Sundrum, Nucl. Phys. B **557** (1999) 79 [hep-th/9810155];
G. F. Giudice, M. A. Luty, H. Murayama and R. Rattazzi, JHEP **9812** (1998) 027 [hep-ph/9810442].
- [41] J. Hisano, K. Ishiwata and N. Nagata, Phys. Rev. D **87** (2013) 035020 [arXiv:1210.5985 [hep-ph]].
- [42] J. Hisano, K. Ishiwata and N. Nagata, Phys. Lett. B **690** (2010) 311 [arXiv:1004.4090 [hep-ph]].

- [43] J. Hisano, S. Matsumoto, M. M. Nojiri and O. Saito, Phys. Rev. D **71** (2005) 015007 [hep-ph/0407168].
- [44] J. Hisano, K. Ishiwata, N. Nagata and T. Takesako, JHEP **1107** (2011) 005 [arXiv:1104.0228 [hep-ph]].
- [45] J. Hisano, D. Kobayashi, N. Mori and E. Senaha, Phys. Lett. B **742** (2015) 80 [arXiv:1410.3569 [hep-ph]].
- [46] D. J. Broadhurst, P. A. Baikov, V. A. Ilyin, J. Fleischer, O. V. Tarasov and V. A. Smirnov, Phys. Lett. B **329** (1994) 103 [hep-ph/9403274].
- [47] W. A. Bardeen, A. J. Buras, D. W. Duke and T. Muta, Phys. Rev. D **18** (1978) 3998.
- [48] A. Djouadi and M. Drees, Phys. Lett. B **484** (2000) 183 [hep-ph/0004205].
- [49] V. A. Novikov, M. A. Shifman, A. I. Vainshtein and V. I. Zakharov, Fortsch. Phys. **32** (1984) 585.
- [50] J. Hisano, K. Ishiwata and N. Nagata, Phys. Rev. D **82** (2010) 115007 [arXiv:1007.2601 [hep-ph]].